Comparing the evolution of debris-free and debris-covered glaciers during the end of the Lateglacial and the Holocene in Dudh Koshi basin, Everest region, Nepal

Vincent Jomelli, Patrick Wagnon, Joanna Charton, Régis Braucher, Leo Martin, Irene Schimmelpfennig, Didier Swingedouw, Deborah Verfaillie, Fanny Brun, Stephanie Gairoard, et al.

Comparing the evolution of debris-free and debris-covered glaciers during the end of the Lateglacial and the Holocene in Dudh Koshi basin, Everest region, Nepal

Vincent Jomelli [a,*], Patrick Wagnon [b], Joanna Charton [a], Régis Braucher [a], Leo Martin [a], Irene Schimmelpfennig [a], Didier Swingedouw [c], Deborah Verfaillie [a], Fanny Brun [b], Stephanie Gairoard [a], Dibas Shrestha [d], ASTER Team [a,1]

[a] *Aix-Marseille University, CNRS, IRD, Coll. France, INRAE, CEREGE, 13545, Aix-en-Provence, France*
[b] *Univ. Grenoble Alpes, CNRS, IRD, INRAE, IGE, F-38000, Grenoble, France*
[c] *Environnements et Paléoenvironnements Océaniques et Continentaux (EPOC), UMR, CNRS, 5805, EPOC-OASU Université de Bordeaux, Allée Geoffroy Saint-Hilaire, 33615, Pessac, France*
[d] *Central Department of Hydrology and Meteorology, Tribhuvan University, Kathmandu, Nepal*

A B S T R A C T

Debris-covered glaciers are very frequent geomorphological features in Khumbu Himal (Nepal). Rock debris on the glacier surface play a significant role in glacier-climate relationships and glacier dynamics. These effects may cause an asynchronous evolution of debris-covered glaciers compared to debris-free glaciers at a multicentennial to millennial scale. Here, we explore this hypothesis by documenting and comparing the multi-millennial Ho-locene evolution of a debris-free glacier, Sabai glacier, and two debris-covered glaciers, Dig and Huuku glaciers, from adjacent catchments in Dudh Koshi basin (Everest region, Nepal). To do so, we dated rock samples collected from moraine boulders on both debris-covered and debris-free glaciers using the ^{10}Be cosmic ray exposure (CRE) dating method. ^{10}Be CRE ages obtained from 41 moraine boulder samples provide time constraints from ~13.5 ka to 0.1 ka. While at Dig (debris-covered) and Sabai (debris-free) glaciers, no moraines from the Lateglacial and the Early Holocene are preserved, debris-covered Huuku glacier evidenced a large glacier extent during the Bølling-Allerød and Early Holocene with two moraines dated respectively to ~13.5 ka and 11 ka, synchronously with most debris-free and debris-covered glaciers in this region. These two glacier advances are concomitant with enhanced monsoon precipitation supporting a qualitative relationship. The absence of debris landforms in the main valley question the nature of Huuku glacier during the Bølling-Allerød and Early Holocene, which could have been either debris-free or covered by a thin debris layer only. During the Mid Holocene, significant dif-ferences are observed in the evolution of the two glacier types. The two debris-covered glaciers recorded a significant advance at ~4.8 ka, synchronous with that observed on other debris-covered glaciers in Khumbu valley. However, such glacier advance during the Mid Holocene was not evidenced on debris-free glaciers in the Dudh Koshi valley. Such a Mid Holocene glacier advance may have a spatial signature with frequent cases re-ported from both types of glaciers in the western part of High Mountain Asia, which are however infrequent in the arid and semi-arid southern and north-eastern Tibet. During the Late Holocene, both types of glaciers evolved similarly again, with moraines spanning the last two millennia, including the Little Ice Age, concomitant with enhanced monsoon precipitation.

1. Corresponding author
E-mail address: jomelli@cerege.fr (V. Jomelli).

[1] ASTER team: Georges Aumaître, Karim Keddadouche, Fawzi Zaïdi.

1.Introduction

Debris-covered (DC) glaciers are widespread in all mountain rangesworldwide (Benn and Owen, 2002; Deline, 2005; Owen and Dortch, 2014; Scherler et al., 2018; Herreid and Pellicciotti, 2020), especially in High Mountain Asia (HMA), where half of the glaciers larger than 2 km2

have more than 5% of their total area covered by a layer of rock debris (Herreid and Pellicciotti, 2020). In some regions of HMA, DC glaciers are even more frequent, such as in the Khumbu Himal (Nepal), where 95% of glaciers larger than 2 km^2 are of the DC type (Herreid and Pellicciotti, 2020). Thus, understanding how debris-covered glaciers may respond to a changing climate is a research priority which feeds into IPCC report recommendations (IPCC SROCC, 2019). To reach this long-term objec-tive, several issues have to be solved and two types of specific studies have to be conducted. First, glaciological surveys have to be maintained to better understand glacier climate relationships at a short time scale and better constrain processes driving mass and energy balance. Second, we need to better understand long-term changes in the extent of these glaciers and associated climate forcings. In this paper we will contribute to this second aspect.

DC glaciers are formed from rock debris delivered to the glacier surface mainly by rockfalls and snow avalanches (Jomelli and Francou, 2000). These rock debris are highly heterogeneous in size, ranging from infra-mm to meter scales, throughout the glacier. This depends on diverse factors such as the size of the glacier or the topography and geology of the catchment (Bhardwaj et al., 2014; Scherler et al., 2011). This debris layer component (thickness and granulometric composition) may vary in time and space at the glacier scale. The evolution of debris thickness is linked to internal debris concentration and glacier mass balance (e.g. Gibson et al., 2017; McCarthy et al., 2021; Compagno et al., 2022), as well as to changes in ice-flow velocity (e.g. Anderson et al., 2021b; McCarthy et al., 2021; Loris et al., 2022). Additionally, external drivers such as rock avalanches may locally control the debris thickness (Berthier and Brun, 2019). Hence, glaciers with negative mass balances tend to increase their debris-cover fractions through time (Mayer et al., 2013; Tielidze et al., 2020). The debris layer has an important control on surface ice melt and glacier retreat (Owen and Benn, 2005; Nicholson and Benn, 2006; Scherler et al., 2011; Rowan et al., 2015; Nicholson et al., 2018; Shokory and Lane, 2023; Giese et al., 2020; Winter--billington et al., 2022). Debris cover is also known to influence the impact of forcings related to radiative heat transfer. It insulates the ice from air temperature fluctuations where the debris cover is thick (~> 10 cm) and continuous, and enhances ablation where the debris cover is thin and discontinuous (Østrem, 1959; Nakawo et al., 1999; Takeuchi et al., 2000; Benn et al., 2003). Some features scattered on DC glaciers, such as ponds, ice cliffs, and streams, locally enhance surface melt (e.g., Benn et al., 2012; Sakai et al., 2002), but are insufficient to overcome the melt-reducing effects of more spatially extensive debris cover (e.g., Anderson et al., 2021).

Due to the insulating effect of thick debris, a decoupling of decadal to centennial variations in solar radiation (Huss et al., 2009) from mass balance could be expected where thick debris cover is present. More-over, the debris layer also influences glacier driving stress and basal sliding, modifying glacier shape and length. This feature is expected to significantly increase the glacier response time (e.g., J óhannesson Raymond and Waddington, 1989; Anderson and Anderson, 2016). For all these reasons it was initially considered that DC glaciers are poorly sensitive to climate change compared to debris-free (DF) glaciers. However, recent investigations of their volume change over the last decades revealed more complex results. Indeed, several studies have shown that DC glaciers exhibit similar thinning rates to debris-free (DF) glaciers in the Himalayas over the recent period (e.g., Kääb et al., 2012; Gardelle et al., 2012; Nuimura et al., 2012; Mölg et al., 2019). The reason is mainly due to the fact that the ablation zones of DC glaciers reach a lower altitude than DF glaciers with enhanced melting rate. Consequently, these recent observations may suggest that DF and DC glaciers would have a comparable evolution, a hypothesis that can be tested over a longer time scale using moraine chronologies.

Based on the effects of the debris layer on the current mass balance and glacier dynamics, one may wonder whether these effects also act on a longer time scale, causing a possible asynchronous evolution of DC compared to DF glaciers. This suggests better addressing glacier-relationships and associated forcings by distinguishing the two types of glaciers at a pluricentennial time scale. The Holocene period, i.e., the last 11,700 years, is appropriate to test such a hypothesis because significant climate changes in HMA have occurred with significant impacts on glaciers (Murari et al., 2014; Saha et al., 2018, 2019a, 2019b). To date, the impact of surface debris cover on glacier evolution during the Holocene remains poorly understood and documented. Some studies in the northern mid-latitudes have mentioned changes in state (Deline, 2005), for example, DF glaciers evolving towards DC after the end of the Little Ice Age (LIA; ~1400–1870 CE; Solomina et al., 2015) or DC glaciers evolving towards rock glaciers (Fernández-Fernández et al., 2017). Other studies have reported a distinct evolution of DC glaciers compared to DF glaciers during the warm Mid Holocene period (8.2-4.2 ka; Fletcher et al., 2023). While DF glaciers in the Alps significantly retreated during this warm Mid Holocene period unfavourable for glacier growth (Jomelli et al., 2022) with glaciers even smaller than 2000 CE in some part, of the Alps (Schimmelpfennig et al., 2022), DC glaciers did not shrink considerably during this period. In some regions they remained stagnant, such as in Iceland (Tanarro et al., 2021). Some divergence in the timing of glacier advance during the Late Holocene (<4.2 ka) has also been observed in sub-Antarctic regions, with asynchronous glacier advance between the two types of glaciers (Charton et al., 2020). However, in HMA, where DC glaciers are very common, especially in the Central and Eastern Himalaya, it remains unclear if they experienced a different millennial time scale evolution than the DF glaciers at the end of the Lateglacial and Holocene, for instance with asynchronous maximum Holocene extent or distinct advance and retreat phases. Several glacier chronologies derived from cosmic ray exposure (CRE) dating have been performed on DC and DF glaciers in HMA (Finkel et al., 2003; Owen, 2009; Barnard et al., 2004, 2006; Murari et al., 2014; Hornsey et al., 2022; Jomelli et al., 2023). Homogenized CRE ages revealed regional divergences depending on the influence of the Westerlies or the intensity of the Indian summer monsoon (Owen et al., 2005, 2008, 2009, Owen and Dortch, 2014; Murari et al., 2014; Rowan, 2017; Saha et al., 2018, 2019a, 2019b). However, direct comparisons between DC and DF glacier chronologies are still lacking and need to be conducted.

The goal of this pilot study is to gain a better understanding of the long-term glacier evolution in HMA during the Lateglacial/Holocene periods. To do so we develop and then compare two DC and one DF ^{10}Be glacial chronologies in the Khumbu Himal (Everest region, Nepal; Figs. 1 and 2) based on 41 rock samples of moraine boulders. These three glaciers were selected from adjacent catchments in order to tentatively minimize possible interferences due to locally varying climatic conditions. The dataset is used to document long-term periods of advance and retreat. These chronologies and their glacier types are then compared against other glacial and climate records in HMA. The study area and climate setting are presented in Section 2. Based on the methodology described in Section 3, the moraine stratigraphy and CRE age results are presented in section 4. In Section 5 we discuss our moraine records and compare the three chronologies with other studies conducted in Nepal and in other regions of HMA, respectively.

2. Study area

2.1. Physical setting

The two DC glaciers and the DF glacier were selected from adjacent catchments and we assumed homogenized climatic conditions on a millennial time scale. Samples from the moraine boulders of these glaciers were collected during field trips that occurred in 2014, 2018, 2019, and 2021. These glaciers are located in the upper Dudh Koshi basin, at about 30 km south of the Everest summit (central Himalaya, 27°74′ N; 86°86’ E) (Figs. 1 and 2). Information about debris cover in this region is available even if the existing glacier and DC inventories (e.g. Herreid and Pellicciotti, 2020) are too coarse to assess the percentage of debris

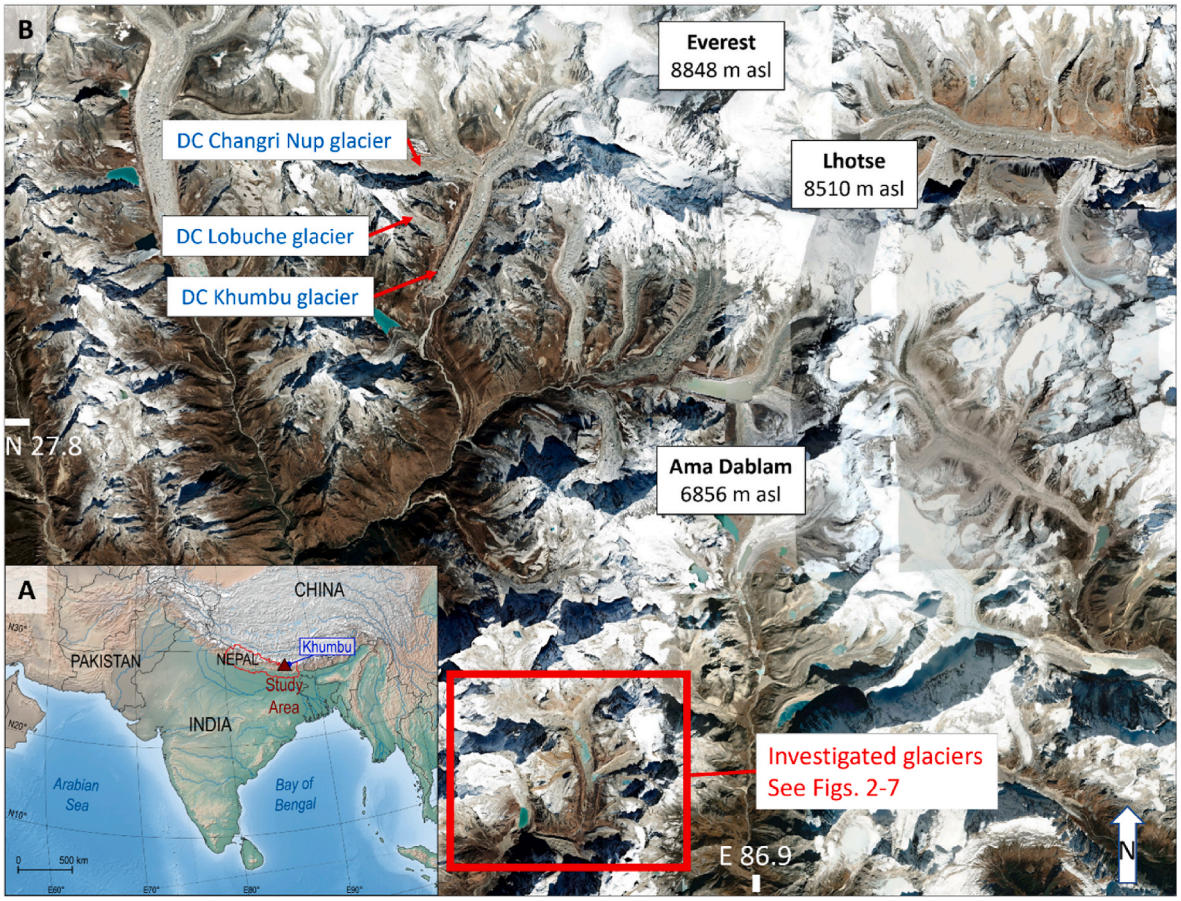

Fig. 1. Location maps. A). The inset shows the study area (red triangle) in High Mountain Asia. B). Debris-free (DF) and debris-covered (DC) glaciers discussed in this study, with the red frame showing the three glaciers investigated in this study.

cover for this area with a satisfying accuracy. These glaciers were selected also because they are connected with two other recently published ^{10}Be chronologies from DF Mera and South Kare glaciers (Jomelli et al., 2023) combined with mass balance observations conducted on Mera glacier over the last two decades (Wagnon et al., 2021). Moreover, this valley is not far from the upper Khumbu valley, where two other published DC chronologies (Hornsey et al., 2022) and glaciological observations conducted on DC Changri Nup glacier (Litt et al., 2019) allow comparisons with nearly comparable climatic conditions.

At the base of a large south-facing amphitheatre of 5 km long, dominated by two large summits, Malangphulang (6573 m a.s.l.) and Kangtega (6685 m a.s.l.), two DC glaciers flow over a length of 3 km, the Huuku Nup and Huuku Shar glaciers. From Herreid and Pellicciotti (2020), the current coverage of Huuku Nup is 48% and 19% for Huuku Shar glacier. The two glaciers meet at about 4900 m a.s.l, at the base of Malangphulang summit, to form the DC Huuku glacier (Figs. 1, 2 and 5). From the confluence, the DC Huuku glacier flows from the north to the south for 2 km towards the Khare settlement. In this part of the catchment, the glacier surface shows numerous supraglacial lakes, ponds and ice cliffs. At about 1.5 km from the confluence, Huuku glacier is coalescent with another smaller DC glacier, the Khare glacier, which flows from Peak 41. Downslope, the surface of the glacier is progressively covered by vegetation and exhibits a hummocky moraine surface that is cut by a river on the right side of the glacier. This vegetated hummocky surface was one of the targets of our sampling sites (Figs. 2 and 3). On both sides of the glacier tongue, two lateral moraine ridges were also selected for our study (Figs. 2–3). These vegetated ridges are separated by 40- 20 m horizontally, and their relief varies between 5 and 20 m. The outermost moraine has a rather flat surface, while the inner one exhibits a more asymmetric cross-profile with a gentler distal side than the proximal side. On the right side of the glacier, the outermost moraine is at least 3 km long. On the left side of Huuku glacier, the two lateral moraines disappear at the connection with moraines formed by two DF Mera and South Khare glaciers that were recently investigated (Jomelli et al., 2023). These two ridges were sampled upstream from the connection.

The second DC glacier investigated in this paper, called Dig glacier (Figs. 1, 2, 4 and 6) by the local people, flows from the north face of Mera summit (6420 m a.s.l.) with an east-west orientation. The upper part of the glacier is composed of a large and steep rock cliff of 2 km in relief between 4600 m and 6300 m a.s.l, partly covered by ice, with several hanging glaciers. The tongue of the glacier starts at the base of the cliff and is 2.5 km long and approximately 550 m wide for most of its length. It has the classic surface features of a DC glacier, with ice cliffs and supraglacial ponds often connected to ice cliffs. From Herreid and Pellicciotti (2020), the current coverage of Dig glacier is 15%. The left side of the glacier at the base of the large rock cliff was not visited, due to risks of serac falls and avalanches. Consequently, the chronology of the DC Dig glacier is based on samples from four lateral moraines on the right side of the glacier that form a large and continuous rampart >50 m in elevation and 2.5 km long. Here, on this rampart, at least one unvegetated and three other vegetated lateral moraines are visible. The unvegetated moraine of about 1–2 m relief is nested with vegetated moraines and is discontinuous for a length of 1 km (Figs. 2 and 4). At some locations on the glacier margin, a vegetated ridge of about 1–2m in relief is 2–5m horizontally away from the unvegetated ridge and was chosen as the best place to tentatively date its deposition. Close to the front of the glacier, two vegetated ridges were selected for our purpose. Here several samples were collected on large and stable boulders on each of these ridges. On the external slope of the rampart, several small

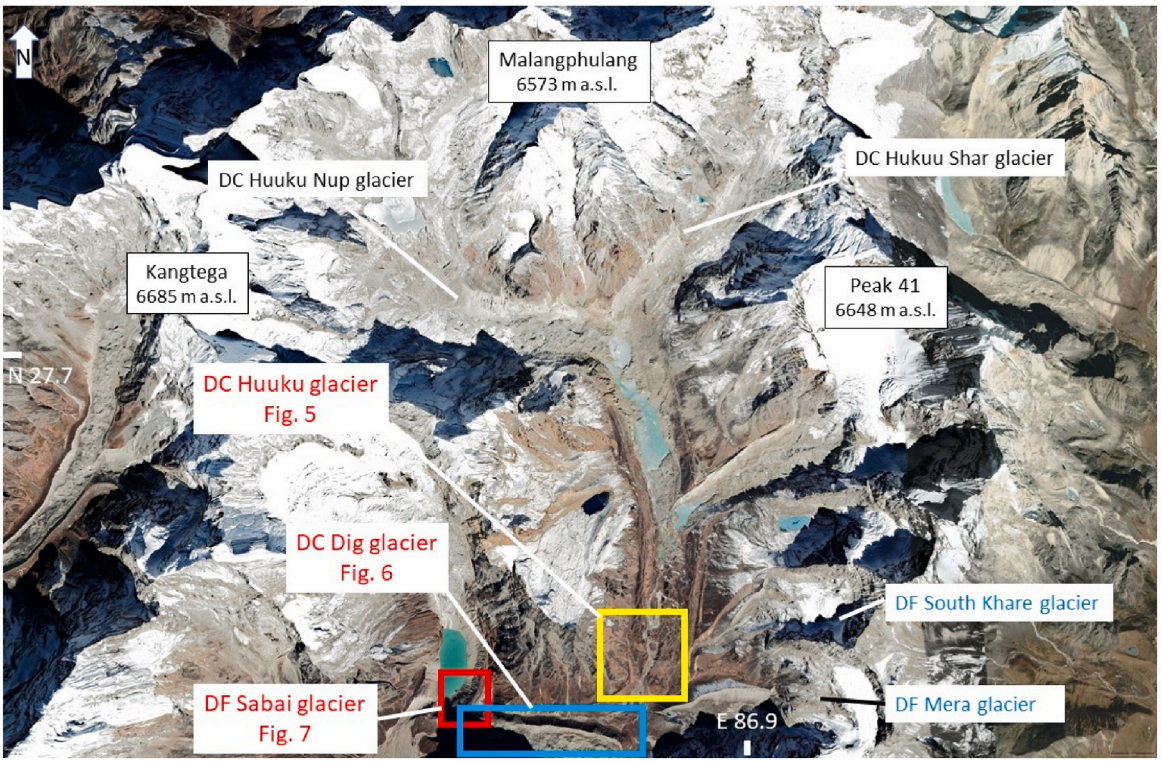

Fig. 2. Zoom on debris-free (DF) and debris-covered (DC) glaciers investigated in this paper. Yellow, blue and red rectangles show areas where samples were collected as presented in Figs. 5–7 respectively.

ridges are visible at different altitudes, but their preservation and their location on the steep slope did not allow us to sample them. Moreover, we can assume that some of them were formed by the merging of several glaciers, including Huuku glacier, which makes their formation rather difficult to interpret.

The last glacier investigated in this study is located 5 km west of the two previous glaciers (Figs. 1, 2 and 4). Sabai glacier (Figs. 1, 2, 4 and 7) is a DF glacier with an area of about 7.5 km^2. It flows southwards from the summit of Kyashar at an altitude of 6770 m a.s.l. The front of the Sabai glacier terminates in the proglacial Tsho Lake behind terminal moraines that formed a massive dam of 200 m high. Part of the right central part of this dam was destroyed by an outburst flood on September 3, 1998 (Osti and Egashira, 2009). Here, we investigated three well-preserved moraines on the left side of the lake at 4500 m a.s.l. (Figs. 2 and 4). Several old moraines visible on the outer slope of the dam were ignored as they were located on too steep slopes.

2.2. Climate setting

The investigated region is under the influence of the Indian Summer Monsoon (ISM), that provides approximately 70% of the annual precipitation falls from June to September (Litt et al., 2019; Perry et al., 2020; Khadka et al., 2022). The mean annual precipitation recorded at Khare at 4888 m a.s.l. is 818 mm (measured over 4 years between 2016 and 2020) and the mean annual temperature is −3.5 °C at Mera La (5350 m a.s.l.) over the 8-year period 2013–2020 (see Table 2 of Khadka et al. (2022) for all meteorological variables measured in this valley). The northern Bay of Bengal is the main source of moisture during the monsoon (62 % of the time in 2019–2020), more than from the Indus River Delta and the Arabian Sea (21 %) and the Indo-Gangetic Plain (17%) (Perry et al., 2020). From October to May, the westerlies on the continent are the predominant moisture source for precipitation (Perry et al., 2020). The monsoon usually stops suddenly at the end of September/beginning of October when the weather turns mostly cloudy, calm and warm. A switch occurs within a few days from frequent precipitation to constantly sunny and dry conditions. Gradually the weather becomes colder and windier, during this post-monsoon period (October–November). Very dry, sunny and windy conditions prevail during the winter (December–February) when clouds or precipitation are almost completely absent. From March to May, the pre-monsoon is characterised by a progressive increase in convective clouds bringing warm and humid air, with a gradually increase in precipitation and a decrease in strong winds (Bookhagen and Burbank D.W., 2006; Sherpa et al., 2017; Khadka et al., 2021).

2.3. Processes controlling the glacier mass balance of debris-free and debris-covered glaciers

2.3.1. Debris-free

In this Indian monsoon-dominated region, ablation is dominated by melt in the lower part of the DF glaciers below the equilibrium line altitude (ELA). Above the ELA, sublimation plays a substantial role during all seasons, except the monsoon (e.g., Wagnon et al., 2013; Stigter et al., 2018; Litt et al., 2019; Fugger et al., 2022; Khadka et al., 2024). Annual and seasonal mass balance measurements on Mera glacier (Fig. 2) conducted over the last decade have revealed that the accumulation and ablation processes happen during the same monsoon period (Wagnon et al., 2021; Khadka et al., 2024). There is limited mass change during the dry, cold, and windy winter, apart from wind ablation and sublimation mainly occurring in the accumulation area (Sherpa et al., 2017; Litt et al., 2019; Wagnon et al., 2021; Khadka et al., 2024). The radiation budget mostly controls the melt (Stigter et al., 2021). The incoming shortwave radiation is maximal during the pre-monsoon, before the installation of permanently overcast conditions during the monsoon, responsible for maximal incoming longwave radiation, compensating the heat loss via outgoing longwave radiation (Bonekamp et al., 2019; Matthews et al., 2020). Overall, the net all-wave radiation is high during the pre-monsoon and monsoon and is controlled by the albedo and by the seasonality of cloudiness (the percentage of cloud in a given atmospheric layer) (Bonekamp et al., 2019; Stigter et al., 2021).

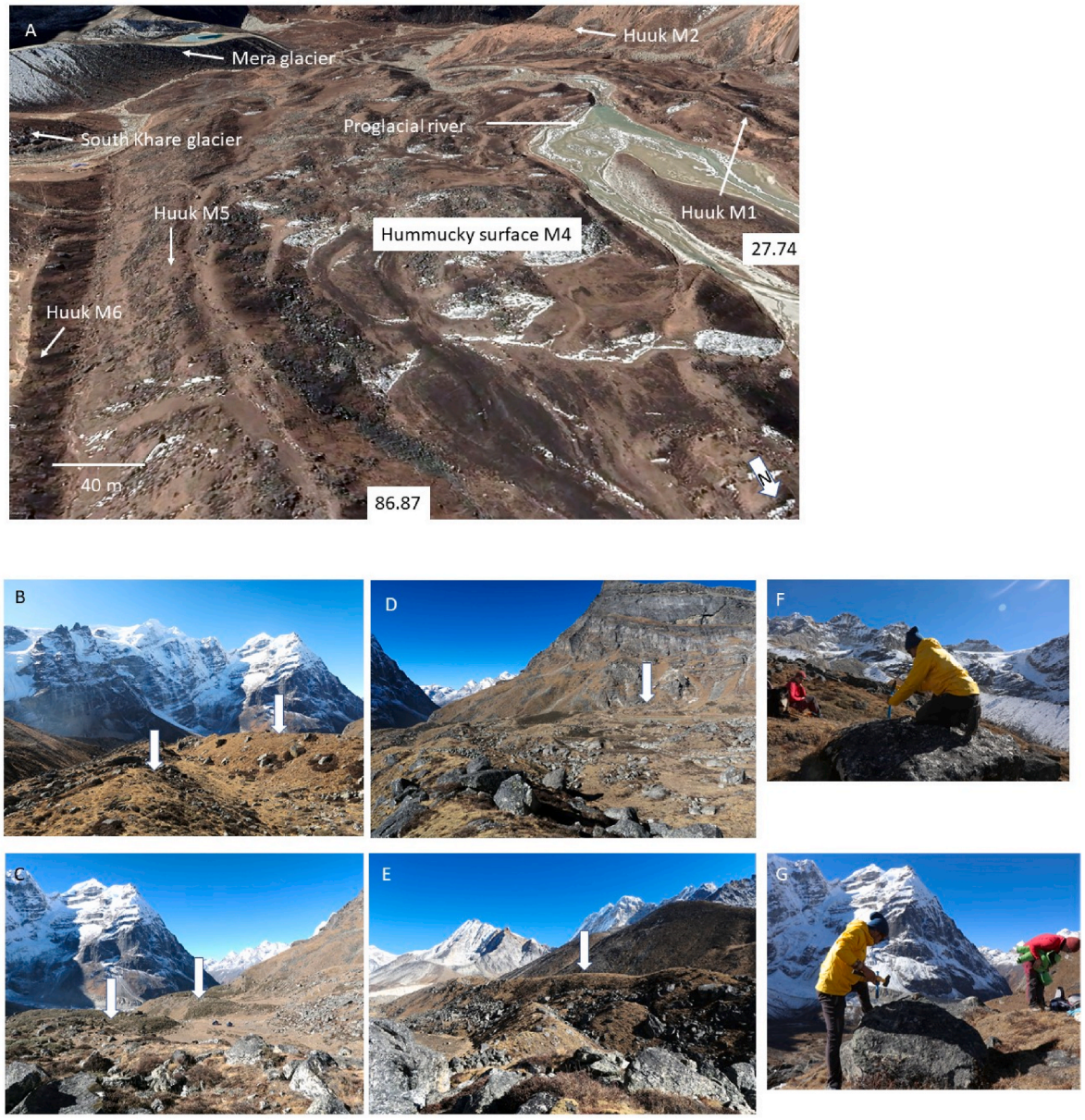

Fig. 3. Photographs of Huuku glacier moraine features. A: General view of Huuku glacier and moraines from Mera and South Kare glaciers. B: left lateral Early and Mid Holocene moraines respectively (white arrows) of about 3–5 m high located close to Mera moraines. In the back the North Face of the Mera Peak; C: Hummocky surface with two hills of about 2–4 m high. The picture is taken from the left side of the glacier towards the right side with Mera peak in the back; D: the hummocky surface and the right Early Holocene moraine of Huuk glacier shown by the white arrow; E: View towards the upper left side of Huuku glacier from the hummocky surface. The white arrow shows the lateral mid Holocene moraine. F, G: sampling on hummocky surface and on right lateral moraine of Huuku glacier.

Wind speed, which influences sublimation, is more important in the accumulation area. Most of the ablation still happens during the monsoon due to stronger melt than during the pre-monsoon season, when refreezing compensates for the melt until the cold content of the glacier surface layers originating from the winter has been evacuated (e.g., Fugger et al., 2022).

2.3.2. Debris-covered

Debris cover has a major impact on the processes that control the mass and energy balance of glaciers and their dynamics. The area covered by debris is restricted to the ablation zone, since any debris falling on the accumulation zone is rapidly buried in the ice and later exposed in the ablation zone. As a consequence, processes prevailing in the accumulation area such as sublimation or wind erosion, are similar for both DC and DF glaciers. The main differences occur over the DC part of the ablation zone. Indeed, the debris cover completely changes the interplay between radiative and turbulent fluxes, on the one hand because the albedo is much lower, and on the other hand because the melting point can be exceeded, leading to unstable conditions during daytime. The main energy source remains the incoming solar radiation which is more efficiently absorbed by the glacier surface, but a large part of this energy is re-emitted towards the atmosphere via outgoing long-wave radiation and a negative and enhanced sensible heat flux (e.g., Giese et al., 2020; Fugger et al., 2022). As a consequence, as long as the debris cover is thin (usually a few centimetres, depending on the type of debris and the local climate), melting is enhanced because the albedo effect prevails over the insulation effect (e.g., Østrem, 1959) but beyond this critical thickness, a large amount of the energy supply at the surface is redirected towards the atmosphere, resulting in less melt on a thick DC surface than over clean ice, and a roughly constant melt over the

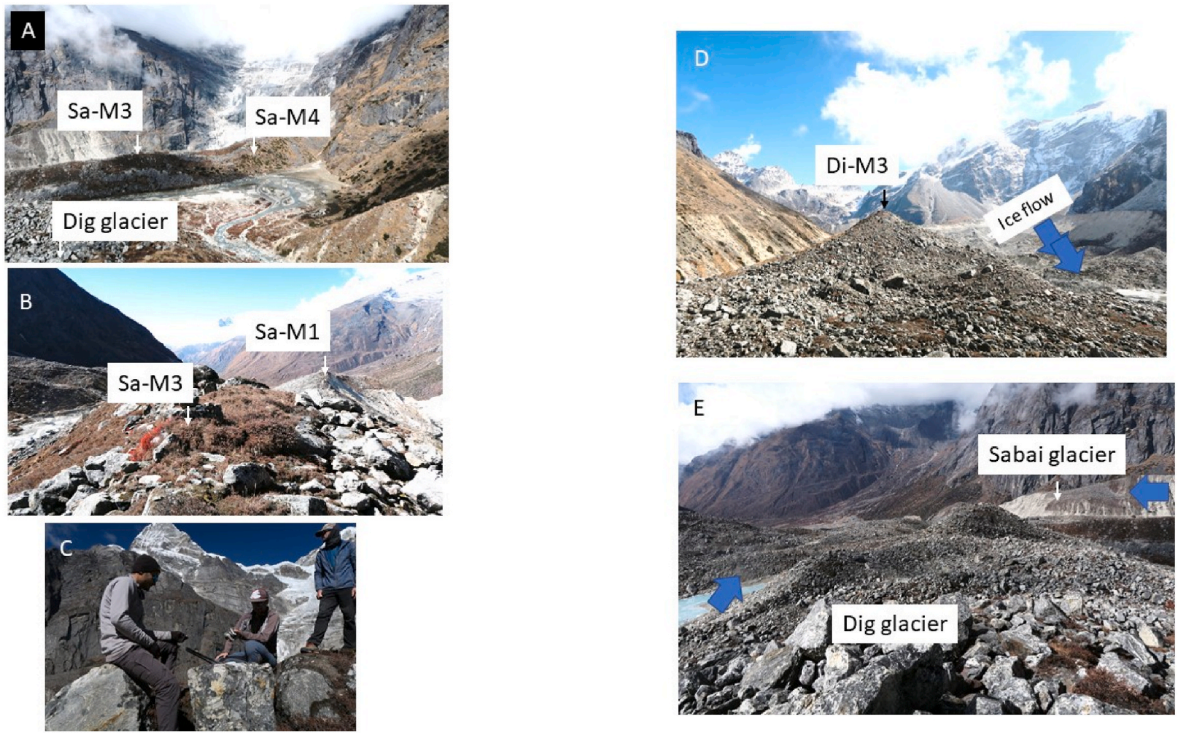

Fig. 4. Moraine features on Sabai and Dig glaciers. A: view of Sa-M3 and Sa-M4 from Dig glacier; B: view of vegetated Sa-M3 and unvegetated Sa-M1 moraines (Sabai glacier); C: sampling on M3-Sa moraine (Sabai glacier); D, E:sampling on hummocky surface and on right lateral moraine of Huuku glacier; F, G: upslope with Mera Peak in the back and downslope views of lateral moraines of Dig glacier, respectively. The blue arrows show ice flow direction.

monsoon period regardless of the meteorological conditions (Fugger et al., 2022). Ablation is very heterogeneous over DC glaciers because of their highly heterogeneous surfaces. Indeed, surface features like ice cliffs or supraglacial ponds have surface properties that are completely different from the surrounding DC areas, and in turn deeply change the surface energy balance. Mainly, melt is increased by a factor of three to ten compared to neighbouring DC surfaces, due to the albedo effect and additional incoming longwave radiation from the surrounding surfaces, and such features are considered as hotspots for melt (e.g., Buri et al., 2016; Miles et al., 2016; Brun et al., 2017). Nevertheless, these ice cliffs and supraglacial ponds have a too limited area and their melting enhancement factors are not large enough to compensate for the reduction in ablation due to debris. As a consequence, DC tongues melt less rapidly than clean ice tongues (Scherler et al., 2011; Nicholson et al., 2018; Anderson et al., 2021b; McCarthy et al., 2921; Winter-Billington et al., 2022).

These surface processes induced by the presence and the development of a debris cover area have strong impacts on the dynamics and the shape of glaciers. Indeed, the debris is exhumed at the surface below the ELA, and the debris layer thickness increases towards lower elevations (Scherler et al., 2011). As a result, melting is very effective in the area closest to the ELA, where debris is thin, and for glaciers that are not in equilibrium with the current climate, this is the area where they experience the greatest thinning. Lower in altitude, as soon as the debris thickness exceeds the Ostrem critical thickness, melt is reduced and therefore DC tongues can be encountered at much lower elevation than those of DF glaciers (Brun et al., 2019). In such an imblance situation, there is less and less ice influx inside the lower part of the glacier resulting in an increasingly stagnant highly DC tongue. Ultimately, due to the increased thinning in the upper part of the thin debris area and the strongly reduced melt over the thick debris lower part, this part may detach from the main trunk of the glacier. Such a situation is commonly observed these days in the Central Himalaya.

In HMA, the sensitivity of glacier mass balance to temperature or precipitation changes has been investigated at a regional scale (e.g., Sakaï and Fujita, 2017; Arndt and Schneider, 2023) or at a glacier scale (Khadka et al., 2024). But to our knowledge, no study has been conducted to compare the mass balance sensitivity to temperature or precipitation between DC and DF glaciers located nearby, and therefore subjected to the same climatic settings. We suspect that, due to the thick debris cover, the investigated DC glacier tongues are better protected from melting and thus less temperature-sensitive than CF tongues. As for sensitivity to precipitation, it is not possible to determine whether it is affected by the presence of debris. As this parameter is assumed to play a key role in controlling long-term glacier change in HMA, new observations are needed before using it as a solid argument that could explain any difference between DC and DF glacier evolution in the past.

3. Methods

3.1. Field sampling

Forty-one granitic moraine boulders (>100 cm in height) were sampled from the crest of the selected moraines (see section 2.1) using a hammer and a chisel. Sample coordinates and elevations were recorded by the handheld Garmin GPS survey instrument (precision 10 m). A Suunto Compass Clinometer PM-5 was used to measure topographic shielding for each sample in the field. We selected boulders on moraines with no evidence of post-glacial disturbance caused by the action of other processes (river, rockfall or debris flow; Jomelli and Francou, 2000). For each glacier investigated, the moraines were named, from the right to the left side of the glacier looking downhill, starting from the youngest M1 to the oldest M_n (Table 1).

3.2. Sample preparation and AMS measurement

All samples were processed at CEREGE (Aix-en-Provence, France). Samples were crushed and sieved to collect the 250–1000 μm fraction. Quartz was first concentrated by magnetic separation and then isolated by successive leaching in a $^{2}/_{3}$ H_2SiF_6 1/3 HCl mixture. The obtained

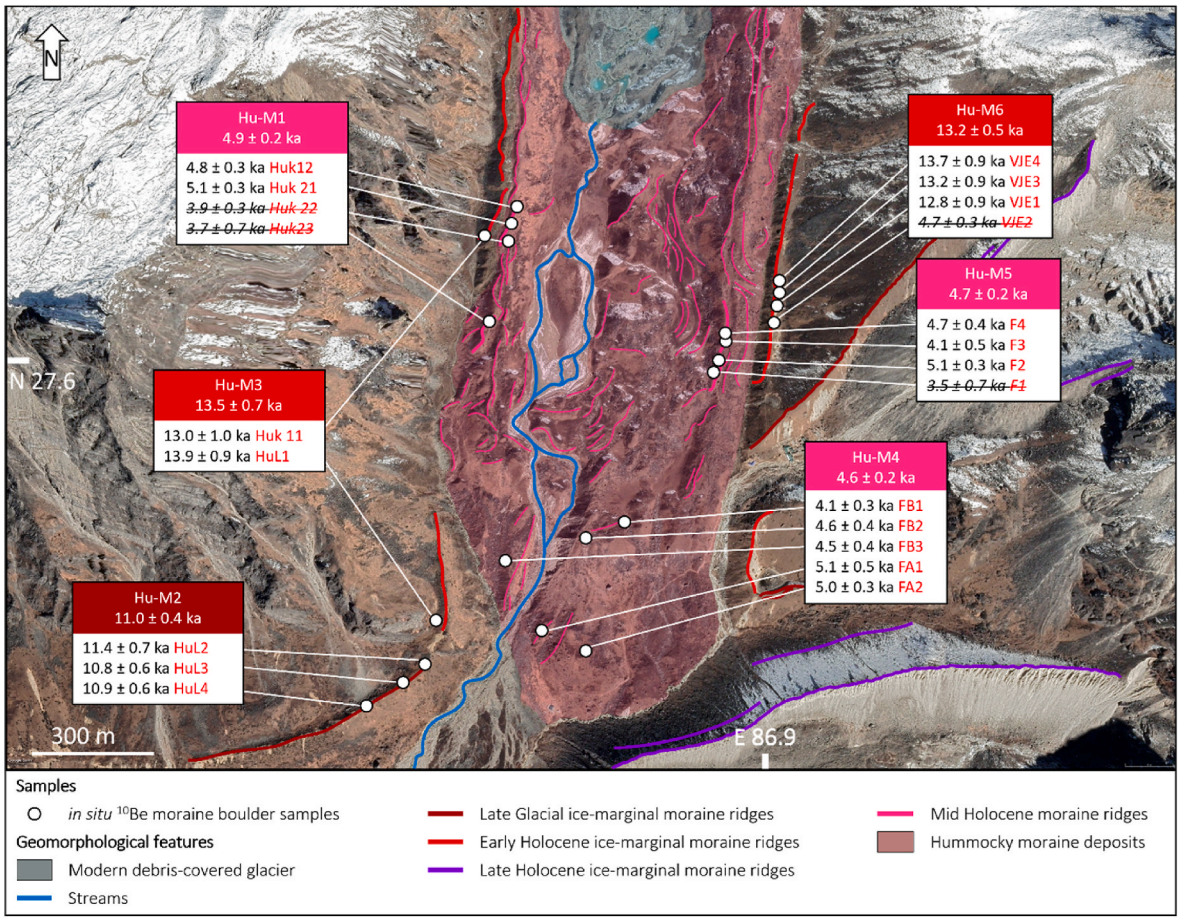

Fig. 5. Chronology of the DC Huuku glacier's evolution. Samples are plotted on an aerial imagery of the investigated glacier. Boxes show the ^{10}Be sample ages of moraine boulders with their external uncertainties. Samples written in striked-through italic text are rejected as outliers and therefore excluded from the discussion. The weighted mean ages for moraine groups are shown in coloured boxes.

quartz fraction was leached at least three times in a 10% HF solution, in order to remove any remaining feldspars and to clean the grains from atmospheric ^{10}Be. Purified quartz was completely dissolved in concentrated HF (48%) after addition of either an in-house ^{9}Be carrier solution (3025 ± 9 ppm; Merchel et al., 2011) or ~450 mg of a ^{9}Be standard carrier solution. Beryllium was extracted by successive alkaline precipitations of $Be(OH)_2$ alternated with separation on anion and cation columns. Samples were then oxidised at 700 °C for 1 h and the final BeO mixed with Nb powder and loaded into copper cathodes. AMS measurements of the ^{10}Be/^{9}Be ratios were conducted at the French national AMS facility ASTER (Arnold et al., 2010). Samples were calibrated against the in-house standard STD-11 (^{10}Be/^{9}Be = 1.191 ± 0.013 *10^{-11}; Braucher et al., 2015) and a ^{10}Be half-life of 1.387 ± 0.0012 * 10^{6} years (Chmeleff et al., 2010; Korschinek et al., 2010). Analytical uncertainties combine ASTER counting statistics, standard uncertainty, external uncertainty (0.5%; Arnold et al., 2010) and machine blank correction. ^{10}Be concentration in the sample was calculated from the corresponding ^{10}Be/^{9}Be ratio and was corrected for associated chemical blanks (Table 1, Table S1, Table S2).

Exposure ages were computed with the online CREp program (Martin et al., 2017; http://crep.crpg.cnrs-nancy.fr) and are listed in Table 1. Scaling to the sample locations was made according to the physically-based LSD model (Lifton et al., 2014) which performs similarly to older empirical models (Borchers et al., 2016). Chosen parameters include the ERA40 atmospheric reanalysis (Uppala et al., 2005) and the VDM (Martin et al., 2017) 2016 geomagnetic database. The global production rate of 4.08 ± 0.23 atoms g^{-1} yr^{-1} was used, as no regional production rate is available so far. Applying the Lal-Stone time corrected scaling scheme (Lal, 1991; Stone, 2000) would rejuvenate the age of about 4–5% (lower than external uncertainties used hereafter). ^{10}Be CRE ages are reported with 1σ "external" uncertainties, which include measurement, production rate and scaling uncertainties (e.g., Balco et al., 2008), in the main text and on the figures (Figs. 5–8) for better comparison with other proxies. Both internal and external uncertainties are reported in Table 1. For a given moraine, its assigned age corresponds to the weighted mean of the sample ages that successfully passed a Chi^2 test (calculated with the internal uncertainties) used to identify outliers (Ward and Wilson, 1978). Here, we preferred the Chi^2 test, as it is more conservative than other tests such as Chauvenet's or Peirce's criteria (Jomelli et al., 2023). Based on field observations, we also considered the stratigraphic relationships to identify outliers.

From a theoretical point of view we may observe some variability in the ^{10}Be ages from a single landform on DC glacier due to boulder pre-exposure during supraglacial transport and post-depositional remobilisation (nuclide inheritance) (Hambrey et al., 2008; Charton et al., 2020). Moreover, the ice-cored moraine melting may cause post-depositional remobilisation that can stretch over several centuries causing another source of variability in the ^{10}Be ages. Nevertheless, we believe that our sampling strategy made it possible to limit the effects of erosion/inheritance on the boulders/moraine surfaces.

4. Results

We present 41 ^{10}Be CRE ages in this contribution. Eight ^{10}Be CRE ages from DC Dig glacier, 22 ^{10}Be CRE ages from DC Huuku glacier and 11 ^{10}Be CRE ages from DF Sabai glacier (Fig. 2). Except for two moraines

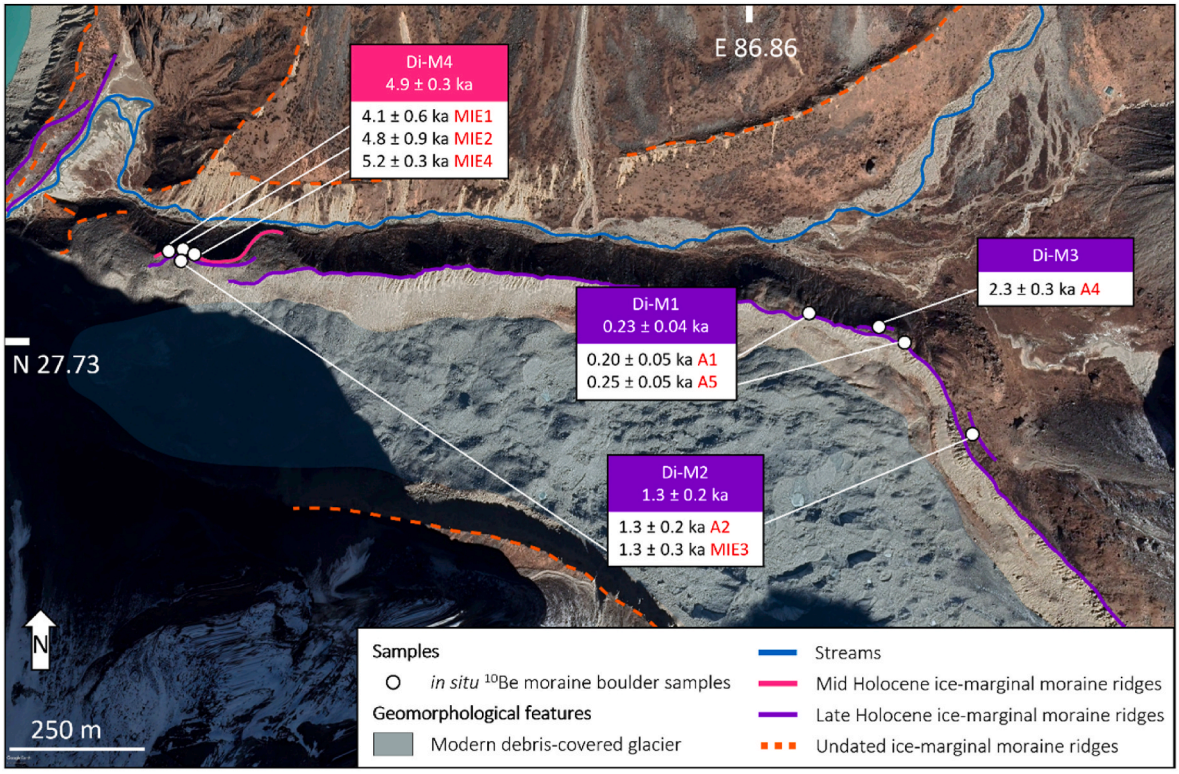

Fig. 6. Chronology of the DC Dig glacier's evolution. Samples are plotted on an aerial imagery of the investigated glacier. Boxes show the ^{10}Be sample ages of moraine boulders with their external uncertainties. The weighted mean ages for moraine groups are shown in coloured boxes.

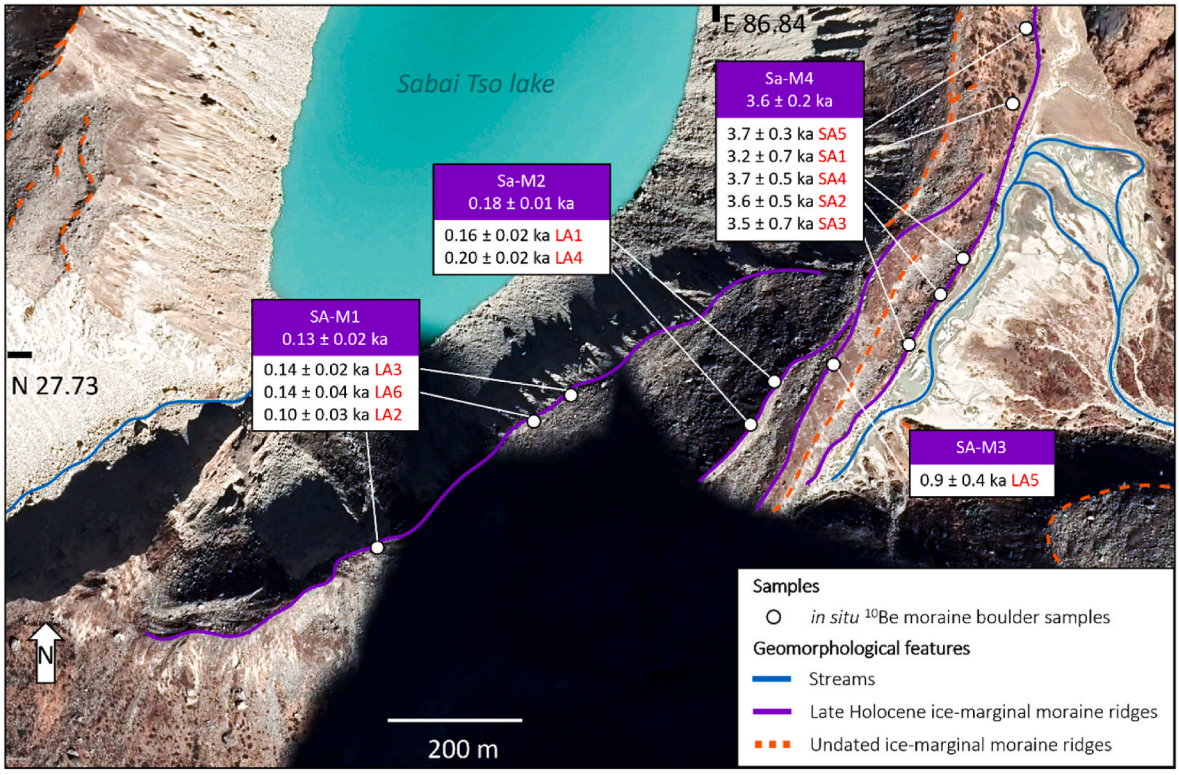

Fig. 7. Chronology of the DF Sabai glacier's evolution. Samples are plotted on an aerial imagery of the investigated glacier. Boxes show the ^{10}Be sample ages of moraine boulders with their external uncertainties. The weighted mean ages for moraine groups are shown in coloured boxes.

Table 1
Cosmogenic data from debris-free and debris covered glaciers. The mean age of the landforms is calculated with external uncertainties.

	Sample ID	Latitude (°N)	Longitude (°E)	Elevation (m a.s.l.)	10Be conc. (at g-1)	10Be uncert. (at g-1)	Shielding factor	Density (g cm-2)	Thickness (cm)	Denudation rate (mmyr-1)	Age (ka)	External uncertainty (ka)	Internal uncertainty (ka)
Debris-covered Huuku glacier n = 22	Mean age right lateral moraine Hu-M1: 4.9 ± 0.2 ka (n = 2)												
	Huk12	27.749612	86.86854	4918	206406	9215	0.9678	2.75	2	0	4.75	0.31	0.18
	Huk21	27.749955	86.86906	4921	231521	7212	0.9678	2.75	3	0	5.12	0.28	0.13
	Mean age right lateral moraine Hu-M2: 10.9 ± 0.3 ka (n = 3)												
	HuL2	27.740079	86.866643	4735	570043	23470	0.9678	2.75	3.5	0	11.41	0.72	0.40
	HuL3	27.739559	86.865842	4728	532631	16544	0.9678	2.75	3.5	0	10.80	0.63	0.28
	HuL4	27.73881	86.864493	4715	534493	18484	0.9678	2.75	3.5	0	10.89	0.64	0.31
	Mean age right lateral moraine Hu-M3: 13.4 ± 0.4 ka (n = 2)												
	Huk11	27.749548	86.86488	4915	717455	36331	0.9678	2.75	3.5	0	13.04	0.96	0.63
	HuL1	27.740191	86.86625	4783	728496	32249	0.9678	2.75	2	0	13.85	0.92	0.54
	Mean age hummocky moraine Hu-M4 : 4.6 ± 0.2 ka (n = 4)												
	FA1	27.740674	86.869702	4741	208830	22587	0.9678	2.75	3.5	0	5.11	0.50	0.44
	FA2	27.740438	86.870938	4751	201851	11214	0.9678	2.75	3.5	0	4.95	0.33	0.22
	FB1	27.74329	86.871921	4806	165371	10082	0.9678	2.75	3.5	0	4.07	0.33	0.23
	FB2	27.742946	86.870843	4807	591073	36883	0.9678	2.75	3.5	0	4.60	0.35	0.25
	FB3	27.742841	86.869041	4787	181763	16280	0.9678	2.75	3.5	0	4.47	0.42	0.35
	Mean age left lateral moraine Hu-M5 : 4.7 ± 0.2 ka (n = 3)												
	F2	27.747081	86.874715	4909	228173	12774	0.98	2.75	3.5	0	5.11	0.34	0.22
	F3	27.747117	86.874745	4909	174340	19385	0.98	2.75	3.5	0	4.05	0.47	0.42
	F4	27.747216	86.874654	4906	205507	15085	0.98	2.75	3.5	0	4.68	0.38	0.29
	Mean age left lateral moraine Hu-M6: 13.3 ± 0.5 ka (n = 3)												
	VJE1	27.748427	86.876276	4919	714252	26345	0.98	2.75	3.5	0	12.75	0.86	0.45
	VJE3	27.748608	86.876225	4908	734642	29412	0.98	2.75	3.5	0	13.22	0.90	0.50
	VJE4	27.749032	86.876326	4922	768944	24712	0.98	2.75	3	0	13.67	0.85	0.39
Debris-covered Dig glacier n = 8	Mean age right lateral moraine Dig-M1: 0.22 ± 0.03 ka (n = 2)												
	A1	27.735003	86.863292	4666	10442	1999	0.975	2.75	3.5	0	0.20	0.05	0.04
	A5	27.734694	86.864624	4685	13017	2395	0.975	2.75	3.5	0	0.25	0.05	0.05
	Mean age right lateral moraine Dig-M2: 1.26 ± 0.15 ka (n = 2)												
	A2	27.732948	86.86652	4679	55454	6835	0.975	2.75	3.5	0	1.25	0.21	0.19
	MIE3	27.736608	86.851388	4529	52947	8715	0.975	2.75	3.5	0	1.29	0.28	0.26
	Age right lateral moraine Dig 2.3 ± 0.3 ka (n = 1) ?												
	A4	27.734668	86.864979	4683	88912	6461	0.975	2.75	3.5	0	2.26	0.26	0.20
	Mean age right lateral moraine Dig-M4: 4.9 ± 0.3 ka (n = 3)												
	MIE1	27.736804	86.851165	4556	146492	22577	0.9678	2.75	3.5	0	4.05	0.62	0.57
	MIE2	27.736754	86.851262	4552	178833	39424	0.9678	2.75	3.5	0	4.83	0.92	0.88
	MIE4	27.736608	86.851388	4529	194670	10152	0.9678	2.75	3	0	5.21	0.33	0.21
Debris-free Sabai glacier n = 11	Mean age left lateral moraine Sa-M1: 0.13 ± 0.02 ka (n = 3)												
	LA3	27.738341	86.845402	4441	6508	755	0.99	2.75	3.5	0	0.14	0.02	0.02
	LA6	27.738236	86.844993	4436	6683	1417	0.99	2.75	3.5	0	0.14	0.04	0.04
	LA2	27.737324	86.84409	4447	4730	1223	0.99	2.75	3.5	0	0.10	0.03	0.03
	Mean age left lateral moraine Sa-M2: 0.18 ± 0.01 ka (n = 2)												
	LA1	27.737939	86.846494	4476	7642	885	0.98	2.75	2	0	0.16	0.02	0.02
	LA4	27.738496	86.846761	4475	9263	828	0.98	2.75	4	0	0.20	0.02	0.02
	Age left lateral moraine Sa-M3: 0.88 ± 0.36 ka (n = 1)?												
	LA5	27.738516	86.847397	4480	38118	13250	0.98	2.75	3	0	0.88	0.36	0.36
	Mean age right lateral moraine Sa-M4: 3.6 ± 0.2 ka (n = 5)												
	SA1	27.740682	86.848998	4479	109675	23339	0.9678	2.75	3.5	0	3.17	0.71	0.68
	SA2	27.738905	86.848128	4479	123357	14353	0.9678	2.75	3.5	0	3.55	0.45	0.39
	SA3	27.73877	86.848044	4482	122213	21098	0.9678	2.75	3.5	0	3.53	0.74	0.70
	SA4	27.739119	86.848384	4476	127790	15571	0.9678	2.75	3	0	3.67	0.50	0.45
	SA5	27.740886	86.849239	4475	127746	7319	0.9678	2.75	2.5	0	3.66	0.29	0.21

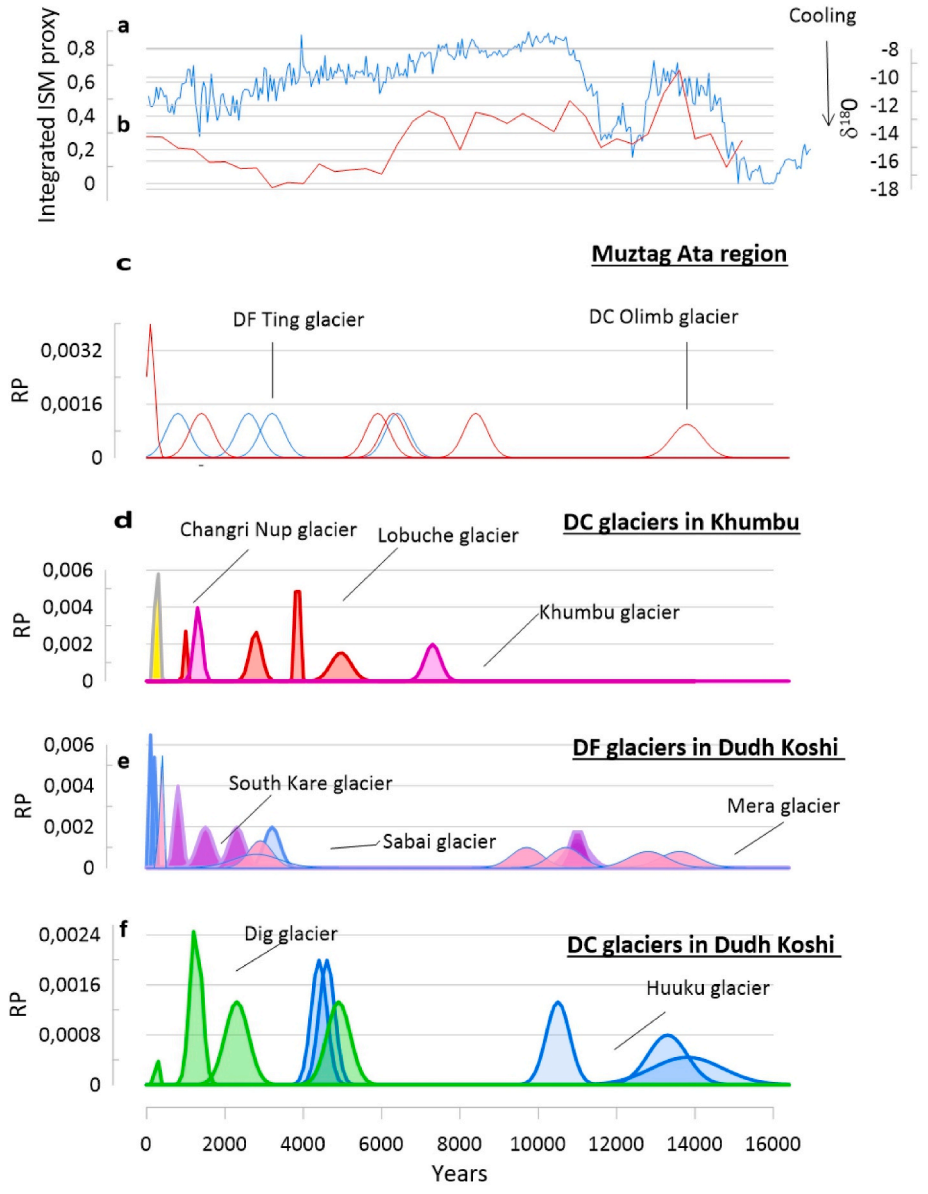

Fig. 8. Normal kernel density functions (i.e., "camelplots") plots for moraines surrounding Dubh Koshi and Khumbu valleys and ISM monsoon proxy record. **a**) Monsoon reconstruction from a compilation of stalagmite d^{18}O from 14 caves (Yu et al., 2022); **b**) Oxygen isotope variations (per mil) from Guliya ice core, Tibet (after Thompson et al., 1997), a proxy for regional temperature; **c**) glaciers change in Muztag Ata region (Tibet-China) expressed as relative probabilities (RP) of density function from CRE chronologies with in blue Debris-free (DF) Ting glacier, and in red Debris-covered DC Olimb glacier after Seong et al. (2009); **d**) Debris-covered (DC) glaciers in Khumbu valley with in pink Khumbu glacier, orange Lobuche glacier and yellow Changri Nup glacier after Hornsey et al. (2022); **e**) Debris-free (DF) glaciers in Dudh Koshi valley with in blue Sabai glacier (this study), in purple South Khare glacier and in pink Mera glacier after Jomelli et al. (2023); **f**) DC glaciers in Dudh Koshi valley with in green Dig glacier and in blue Huuku glacier (this study).

that were tentatively dated using a single sample and stratigraphy, the other moraine ages were based on between two and four samples.

4.1. *Debris-covered Huuku glacier chronology*

At about 2 km south of the confluence of Huuku Nup and Huuku Shar glaciers, samples were collected on three moraine ridges on the right side of the Huuku (Hu) glacier, on one hummocky surface in the middle of the valley and on two lateral moraines on the left side of the glacier (Figs. 2, 3 and 5).

Close to the confluence on the right side of the glacier, two distinct vegetated ridges are visible about 1 km in length with an elevation ranging from 5000 to 4900 m a.s.l. These two ridges are located about 50 m from each other. Four samples Huk12, Huk21, Huk22, Huk23 were collected on the moraine clostest to the iceflow. These samples can be separated into two subgroups. Huk22 dated to 3.9 ± 0.3 ka and Huk23 dated to 3.7 ± 0.7 ka yield a^{10}Be CRE weighted mean age of 3.9 ± 0.2 ka. These two samples are younger than the two other ones Huk12 dated to 4.8 ± 0.3 and Huk21 dated to 5.1 ± 0.3 ka. The two youngest ages were considered here as outliers yielding to Huk-M1 a mean of 4.9 ± 0.2 ka (n = 2). About 2 km from the confluence the valley changes from a north-south to an east-west orientation and one long ridge of about 50 m in relief, Hu-M2 is visible. On the top of it, three samples (HuL2, HuL3 and HuL4) with ages ranging from 10.8 ± 0.6 to 11.4 ± 0.7 show a good consistency and give a^{10}Be CRE weighted mean age of 11.0 ± 0.4 ka (n = 3).

The highest and most external ridge on the right side of the glacier Hu-M3 was dated to 13.5 ± 1.0 ka (n = 2) based on the weighted mean

of two sample ages Huk11 and HuL1. Huk11 was collected on the uppermost part of the moraine ridge. HuL1 was collected downstream and on the external part of another crest of the old-ridge Hu-M3. As the age of HuL1 is similar to the age of Hu11 of ~13 ka we assume these two moraine remains correspond to the same glacial advance.

In the middle of the valley, a hummocky surface, labelled Hu-M4, about 0.5 km long and with a relief of about 2–5 m lies in between lateral moraines from both sides of Huuku glacier. The left side of this hummocky surface is also constrained by a frontal moraine from two other DF glaciers, South Khare and Mera glaciers, respectively (Figs. 3 and 5). Here, five samples were collected on different hills that form this Hu-M4 hummocky field. These samples FA1, FA2, FB1, FB2, FB3 yield ages of 5.1 ± 0.5 ka, 5.0 ± 0.3 ka, 4.1 ± 0.3 ka, 11.4 ± 0.9 ka and 4.5 ± 0.4 ka, respectively. FB2, dated at 11.2 ± 0.7 ka, is considered as an outlier based on the Chi^2 test and therefore excluded from the mean age calculation of Hu-M5, resulting in a weighted mean age of 4.8 ± 0.2 ka (n = 4).

Northeast of this hummocky landform, two large vegetated moraines located on the left side of the glacier were investigated. On the inner-most Hu-M5 moraine, four large boulders (F1, F2, F3, F4) were selected. One slightly younger sample (F1) did not pass the Chi^2 test and is therefore excluded from the weighted mean calculation. The other samples yield a weighted mean age of 4.7 ± 0.2 ka (n = 3). Finally, four samples (VJE1, VJE2, VJE3 and VJE4) were collected on the long and outermost ridge Ku-M6 upstream from the connection with a right lateral moraine of the DF South Khare glacier. VJE2, dated at 4.7 ± 0.2 ka, is considered as an outlier based on the Chi^2 test and is therefore rejected from the mean age calculation of Hu-M6, which gives a weighted mean age of 13.2 ± 0.5 ka (n = 3).

4.2. Debris-covered Dig glacier chronology

The chronology of the DC Dig (Di) glacier is based on eight samples from four lateral moraines on the right side of the glacier (Figs. 2, 4 and 6). The first Di-M1 unvegetated moraine corresponds to a narrow ridge on the innermost part of the rampart. While the inner part of the ridge is mostly unstable and eroded, the outer part of it is gentler and more stable. However, to avoid possible remobilisation, boulders were selected on the crest. The two boulders located at about 1 km from the base of the cliff give ages of 0.20 ± 0.05 ka (A1) and 0.25 ± 0.05 ka (A5), yielding a weighted mean age of 0.23 ± 0.04 ka (n = 2). At a horizontal distance of a few metres from Di-M1, another ridge Di-M2 with approximately the same relief is partly covered by vegetation. A first sample A2 with a ^{10}Be CRE age of 1.3 ± 0.2 ka was selected close to the previous samples A1 and A5, located on the innermost ridge. The other sample MIE3, dated at 1.3 ± 0.3 ka, was selected closer to the front and is assumed to be on the same ridge, giving to Di-M2 a weighted mean age of 1.3 ± 0.2 ka (n = 2). Close to the samples collected on Di- M1, one sample A4 was selected on another embedded vegetated ridge, Di-M3, located on the outer part of the rampart and yield a ^{10}Be CRE age of 2.3 ± 0.3 ka. Finally, close to the front, three samples MIE1 (4.1 ± 0.6 ka), MIE2 (4.8 ± 0.9 ka), and MIE4 (5.2 ± 0.3 ka) were collected on the top of the outermost rampart, the Di-M4 ridge. This Di-M4 ridge yields a weighted mean age of 4.9 ± 0.3 ka (n = 3).

4.3. Debris-free Sabai glacier chronology

The chronology of the DF Sabai (Sa) glacier is based on 11 samples from four lateral moraines on the left side of the glacier (Figs. 2, 4 and 7). These moraines form a large vallum of 80 m in relief behind which the large proglacial lake Sabai Tso is visible. Sa-M1 corresponds to a latero-frontal unvegetated ridge of about 1–2 m in relief at the top of the vallum. A small moraine ridge is visible on the innermost side of the vallum, but is inaccessible. On Sa-M1, three samples LA2, LA3 and LA6 give ^{10}Be CRE ages ranging from 0.10 ± 0.03 ka to 0.14 ± 0.04 ka, yielding a weighted mean age of 0.13 ± 0.02 ka (n = 3). On the distal slope of the rampart, embedded in Sa-M1, another ridge, Sa-M2, is visible with a relief of 1–2 m over 100 m. Here, two samples LA1 and LA4, from boulders partly covered by small lichens, yield a weighted mean age of 0.18 ± 0.01 ka (n = 2). On the left side of the rampart, two larger and higher vegetated moraines are visible. The crest of the highest one (Sa-M3) is 2 m high and 200 m long and has an asymmetric transversal profile with a steeper proximal slope. On this Sa-M3 ridge, one sample LA5 was taken, yielding an age of 0.9 ± 0.4 ka. At about 20 m horizontally from Sa-M3, the outermost Sa-M4 ridge investigated in this study is totally vegetated and has a gentle surface. This ridge has a relief of 5 m and a length of over 400 m. Here, the five samples SA1 to SA5 give consistent ^{10}Be CRE ages yielding a weighted mean age of 3.6 ± 0.2 ka (n = 5).

5. Discussion

5.1. Evolution of the debris-covered Huuku and Dig glaciers during the Lateglacial and Holocene

Spanning ~13.5 ka, this new ^{10}Be CRE age dataset from moraine boulders provides time constraints for the DC Huuku and Dig glaciers. It also helps to improve our knowledge about the evolution of DC glaciers in this region during the Lateglacial and the Holocene. The oldest evidence of glacier advance is recorded at the base of Huuku Glacier, where dating at both sides of the glacier (left lateral moraine Hu-M6 and the right lateral moraine Hu-M3) reveals a large glacier extent at ~13.2 and ~13.5 ka, respectively, most likely during the Bølling-Allerød (B/A; 14.7 - 12.9 ka) warm event. The size of the glacier during this advance is unknown, but the glacier reached a length of at least 1.5 km from the change in valley orientation. Interestingly, this advance during the B/A coincides with an excess of precipitation (but not the Lateglacial-Holocene maximum precipitation) in the region documented by a continuous integrated ISM proxy record (Fig. 8). This proxy is a compilation of stalagmite δ^{18}O data from 14 different caves spanning 0–35N, 70-95E (Yu et al., 2022). Interestingly, the B/A is known to be a warmer period than the Younger Dryas (YD: 12.9-11.7 ka) in the northern Hemisphere but cooler than the Holocene. However, δ^{18}O record from the Guliya ice core (Thompson et al., 1997) shows warmer conditions than during the Holocene. Since we did not find evidence of moraine formation during the YD we thus may suspect these glaciers were more sensitive to precipitation than to temperature during the Lateglacial-Holocene transition.

Subsequent glacier advance occurred during the Early Holocene, as indicated by the direct dating of the Hu-M2 moraine at ~11 ka on the Huuku glacier forefield. This Early Holocene moraine represents the Holocene maximum extent of our dataset, which is also concomitant with the maximum Holocene precipitation but warmer temperatures in the region (Fig. 8). During this period, two DF glaciers, Mera and South Khare, with similarly large advances, may have merged with Huuku Glacier, as suggested by the shape of their respective lateral moraines (Fig. 2). It is noteworthy that the Lateglacial and Early Holocene evolution of DC Dig Glacier could not be documented due to the lack of moraine preservation.

From ~11 to 4.8 ka, the evolution of the Huuku and Dig glaciers is unknown. Although ISM precipitation remains high and regional temperature is still warmer than during the Late Holocene, we have not found evidence of moraine formation during the Mid Holocene. We can assume that the front of the two glaciers was upslope from the Late Holocene advances. On the two DC Huuku and Dig glaciers, a synchronous large advance occurred at the transition between the Mid and the Late Holocene, at ~4.7 ka, as evidenced by moraines Hu-M1 (4.9 ± 0.2 ka) and Hu-M5 (4.7 ± 0.2 ka) on Huuku glacier and moraine Di-M4 (4.9 ± 0.3) on Dig glacier. The climatic origin of this advance remains unclear, as a peak in the ISM dated to 3.9 ka postdates the formation of the moraines (Fig. 8). The formation of the hummocky surface Hu-M4 on Huuku glacier dated to ~4.8 ka, with its lateral moraine Hu-M5, may

reveal the position of the glacier front at this time (Fig. 5). One can also notice a good consistency of the sample ages with only few outliers, suggesting that the surface stabilised rapidly with limited inheritance of the boulders. Interestingly, this type of hummocky surface is not observed downstream, questioning the homogeneity of the thickness of the DC layer on Huuku glacier or even the nature of the glacier, which could have changed from DF to DC type throughout the Holocene. Indeed, downslope of the hummocky surface where Lateglacial and early Holocene moraines are observed, the valley does not show any surface that would correspond to an old tongue of a DC glacier. Thus, it could be supposed that Huuku glacier had a thin DC layer or even no debris cover during the Lateglacial-Early Holocene. Otherwise we as-sume that some remains would be visible downslope from the hummocky surface. This debris cover may have increased during the Mid-Late Holocene due to the disconnection of the two DF Mera and South Khare glaciers, and possible changes in climatic conditions. Indeed, the connection of two DF glaciers with Huuku glacier in the Early Holocene would have increased the clean ice flow in the catchment, favoring a debris-free tongue. Later, the glaciers would have separated. The rock debris/clean ice ratio would have changed drastically, favoring the formation of a DC glacier type.

During the Late Holocene, the evolution of the Huuku glacier remains unknown, while the DC Dig glacier shows at least two advances at ~2.3 and ~1.3 ka and during the LIA, associated with enhanced ISM strength and strong variability associated to progressive warmer conditions in this region.

5.2. Comparison with other debris-covered and debris-free glaciers in Khumbu region

Comparison of the evolution of the two DC glaciers in the Dudh Koshi valley with other glaciers in the region reveals intriguing results (Fig. 8). Huuku glacier experienced a similar advance during the B/A as previously observed on the DF South Khare glacier in the same valley (Figs, 1–2) (Jomelli et al., 2023). Both glaciers show a maximum Holocene glacier advance at ~11-10.8 ka, as also observed on the other DF Mera glacier (~11 ka; Jomelli et al., 2023). However it remains difficult to conclude if DF and DC glaciers in the Dudh Koshi valley had a synchronous millennial evolution during the B/A and Early Holocene periods as we wonder if Huuku glacier was a DF glacier during the B/A and Early Holocene. Interestingly, Hornsey et al. (2022) suggested that such a major Early Holocene advance occurred on Khumbu glacier. However, such an advance was not observed on another DC Lobutche glacier located close to Khumbu glacier (Hornsey et al., 2022).

At the end of the Mid Holocene, there were significant differences between the two types of glacier evolution. The two DC glaciers in this study experienced a significant advance, or their front remained stable, as evidenced by the formation of the hummocky moraine at ~4.8 ka on Huuku glacier. Interestingly, this late Mid Holocene glacier pattern is broadly synchronous with that observed on DC Lobuche glacier in the Khumbu valley (Hornsey et al., 2022, Fig. 8), but younger than the Mid Holocene moraine recorded on Khumbu Glacier at ~7 ka (Fig. 8). However, such a late Mid Holocene advance has not been recorded on DF glaciers in this region. One may suspect that such a difference may be related to different response times or due to the fact that the position of the front of DC glaciers did not change as much as that of DF glaciers as observed today, due to warmer climate conditions. On the Khumbu glacier, Hornsey et al. (2022) showed a major shift in dynamic behaviour between the Early and Mid Holocene, from a change in terminus position in the Early Holocene to thickening of the ablation area to build a closely spaced set of moraines through subsequent glacial stages during the Mid and Late Holocene (Delaney and Anderson, 2022). Here, a comparable pattern is observed on the two DC glaciers with embedded moraine crests from the Mid Holocene on Dig glacier and the formation of a hummocky moraine on Huuku glacier.

In contrast, such glacier advance during the Mid Holocene was not evidenced on DF glaciers in the upper Dudh Koshi basin. Even if on DF Sabai glacier poorly preserved moraines visible at the base of the front may hypothetically correspond to this period, robust evidence of a glacier advance during the Mid Holocene is not observed on DF Mera and South Khare glaciers. Thus, the Late Holocene advances of DF glaciers may have overridden the deposits of previous shorter Mid Holocene glacial extents (if any), while the dynamics of DC glaciers did not but created embedded crests instead. Climatic and dynamic causes of these changes would require specific analyses based on robust modelling approaches that are out of the scope of this paper but are definitely an avenue for future research. One may assume that despite wet and warm conditions during the Mid Holocene, the ablation zone of DC glacier tongues in Khumbu region were preserved at low altitudes due to the insulating debris cover, while DF glacier tongues shrunk due to enhanced melting.

During the Late Holocene, glacier advances are evidenced on both types of glaciers. DF glaciers experienced a large advance at ~3.6 ka evidenced by dated-moraines such as Sa-M4 on Sabai glacier (Fig. 8), which is also observed through moraine formation on DC Lobuche glacier in the Khumbu valley (Fig. 8) (Hornsey et al., 2022). Climate conditions during the Late Holocene would have favoured a large glacier advance and thickening of the ablation area in the case of DC glaciers behind Mid Holocene moraines as evidenced at the base of Khumbu glacier (Hornsey et al., 2022). From this maximum Late Holocene advance, both types of glaciers experienced minor advances, in particular during the onset of the last millennium and the LIA (Solomina et al., 2015, 2016). On DF Sabai glacier for instance two moraines were formed during the LIA synchronously with those recorded on the other DF Mera and South Khare glaciers and DC Dig, Kumbu and Lobuche glaciers (Fig. 8; Hornsey et al., 2022; Jomelli et al., 2023).

5.3. Glacier type versus other factors that influence their fluctuations

Addressing the question of the evolution of DC glaciers during the Holocene from a limited number of glaciers remains difficult. Additional glacier chronologies are needed to better constrain their evolution. This would help identifying the role of geomorphological parameters on glacier fluctuations. Indeed, it is now well known that geomorphological characteristics of glacier catchment have a strong influence on current glacier mass balance (Barandun and Pohl, 2022; Guha and Tiwari, 2023). For instance, Brun et al. (2019) evidenced that a stronger melting rate than the regional average over the last decades is observed for glaciers with a flatter tongue slope or when the tongue is connected to a proglacial lake. Conversely, the aspect of the accumulation area does not play any significant role on mass balance variability. However, the influence of the geomorphological context on glacier mass balance at pluridecadal, centennial or even millennium time scales remains poorly constrained. We may suspect that some geomorphological parameters would still have a strong influence while others would not. Such influence may be responsible for the asynchronous glacier response to climate change which needs to be further investigated.

Moreover, it is well known that glacial erosion, weathering, debris supply, climate and weather conditions and glacier dynamics all affect the evolution of debris cover. However, any change in the evolution of debris cover might have a strong impact on the glacier-climate relationship. A limited factor in our investigation therefore arises from the complication that such changes can operate over a few decades (rapidly changing environment) to several centuries (slightly more stable conditions), while the moraine records document changes mostly on the millennial timescale. Observations from New Zealand (Kirkbride, 1993) and the European Alps (Deline, 2005) show that, following the LIA, some valley glaciers significantly increased their debris cover, thereby forcing a different and often lower response to warming compared to DF glaciers. In this study the question of a possible synchronous major advance during the early Holocene between DF and DC glaciers remains to be addressed as we suspect Huuku glacier not to be a “true” DC glacier

at that time. All in all, new investigations on glacier fluctuations focusing on different time scales are needed to better understand glacier-climate relationship in HMA including the question of the nature of the investigated glaciers.

5.4. A possible spatial signature of the Mid Holocene glacier advance in HMA

Saha et al. (2019a) classified himalayan glaciers according to five climatic zones in HMA based on spatial variability of temperature and precipitation. Considering their description, it is interesting to note that this Mid Holocene glacier advance may have a spatial signature. Indeed, it seems to be rare in eastern Himalaya and exclusively related to DC glaciers. To date, only one case has been reported so far from another DC glacier in Langtang (Barnard et al., 2006). This 4-5 ka Mid Holocene glacier advance is also very rare in the arid and semi-arid climatic zones of southern and north-eastern Tibet (Saha et al., 2019a), regardless of the type of glacier. In contrast, such a glacier advance was observed much more frequently in the western part of HMA, including wet temperate central Himalaya, transitional western Himalaya and western Tibet. In these regions, such an advance was documented on both types of glaciers. For instance, Saha et al. (2018) report an advance of DF Gomuche glacier dated to ~4.4 ka while Seong et al. (2009), reported an advance of DF glaciers in Muztagh Ata and Kongur Shan near Tajikistan at the end of the Mid Holocene (Fig. 8). Local glacial advances also occurred in other areas of Zanskar, e.g., in the Puga valley (Hedrick et al., 2011) in the mid-latitude westerlies dominated Central Kar-akoram (Seong et al., 2007). Thus, this Mid Holocene glacier advance would be more of a signature of the influence of changes in the "west-erlies" rather than changes in the monsoon regime, where it would only be preserved on DC glaciers such as in Khumbu. Interestingly, such advances coincide with decreasing strength of the Atlantic Meridional Overturning Circulation (AMOC) from the Mid Holocene, inducing cooler conditions in the Northern Atlantic regions and enhanced westerlies (Thornalley et al., 2013; Ayache et al., 2018; Jomelli et al., 2022). However, climate forcings responsible for such evolution in the Khumbu region remain difficult to elucidate, as a direct quantitative relationship between monsoon variations documented from proxy records or climate model results does not perfectly match with glacier fluctuations documented from moraine records as previously evidenced (Jomelli et al., 2023).

6. Conclusion

The main goal of this paper is to compare the evolution of DF and DC glaciers during the end of the Lateglacial and the Holocene in central Himalaya. For that reason, we investigated the evolution of two DC (Huuku and Dig) glaciers and one DF (Sabai) glacier during the end of the Lateglacial and the Holocene in the upper Dudh Koshi basin based on 41 ^{10}Be CRE ages of samples collected from boulders on moraines. These chronologies were compared to other published chronologies derived from ^{10}Be CRE ages from both DF and DC glaciers located in the same valley and in other HMA regions. Although the lack of Lateglacial and Early Holocene moraines did not permit investigating Dig and Sabai glacier changes during these periods, Huuku glacier experienced a large glacier extent during the Bølling/Allerød and Early Holocene synchronously with several DF and DC glaciers in this region. As we discuss the nature of Huuku glacier during the Bølling/Allerød-Early Holocene periods it is too early to conclude to a comparable millennium-scale advance period for both types of glaciers in this part of the Himalaya. Significant differences were observed between both types of glaciers during the transition of the Mid-Late Holocene, while a comparable evolution was evidenced again during the Late Holocene. During the Mid Holocene, a glacier advance was recorded from most DC glaciers in the Khumbu region, while moraines dated to this period at the base of DF glaciers have not been found yet. Either DF glaciers were retreating at this time or larger advances during the Late Holocene recovered previous Mid Holocene remains. However, such a Mid Holocene glacier advance may have a spatial signature, that may reflect specific climatic conditions rather than the nature of the glacier. Such a Mid Holocene glacier advance would be observed for both types of glaciers in the western part of HMA but would be rare in other regions and better preserved at the base of DC glaciers in Dudh Koshi valley.

Author contributions

V.J. designed the paper. V.J., PW., F.B., and D. S, realized the field sampling, R.B., J.C., A.H., S.B and V.J. processed the 10Be sample preparation and analysis. V.J., R.B., J.C., A.H., S.B and ASTER TEAM computed the cosmogenic nuclides ages. V.J. wrote the first draft of the paper and all authors contributed to the discussion and final version of the manuscript.

Declaration of competing interest

The authors declare that they have no known competing financial interests or personal relationships that could have appeared to influence the work reported in this paper.

Acknowledgments

The ASTER AMS national facility (CEREGE, Aix-en-Provence) is supported by the INSU/CNRS, the ANR through the "Projets thematiques d'excellence" program for the "Equipements d'excellence" ASTER-CEREGE action and IRD. Sample cost was granted by Evereth project supported by the French National program LEFE (Les Enveloppes Fluides et l'Environnement). Field work, and mass and energy balance results have been supported by the French Service d'Observation GLACIOCLIM, part of IR OZCAR. This work would not have been possible without the support of the IRD International Joint Lab WATER-HIMAL (PIs: D. Shrestha, and P. Wagnon) and all the efforts from people in the field: porters, students, helpers, colleagues who are greatly acknowledged here.

Appendix A. Supplementary data

Supplementary data to this article can be found online at https://doi.org/10.1016/j.quascirev.2024.108994.

Data availability

Data will be made available on request.

References

Anderson, L.S., Anderson, R.S., 2016. Modeling debris-covered glaciers: response to steady debris deposition. Cryosphere 10 (3), 1105–1124. https://doi.org/10.5194/tc-10-1105-2016.

Anderson, L.S., Armstrong, W.H., Anderson, R.S., Buri, P., 2021. Debris cover and the thinning of Kennicott Glacier, Alaska: in situ measurements, automated ice cliff delineation and distributed melt estimates. Cryosphere 15 (1), 265–282. https://doi.org/10.5194/tc-15-265-2021.

Anderson, L.S., Armstrong, W.H., Anderson, R.S., Scherler, D., Petersen, E., 2021b. The causes of debris-covered glacier thinning: evidence for the importance of ice dynamics from Kennicott glacier, Alaska. Front. Earth Sci. 9, 723. https://doi.org/10.3389/FEART.2021.680995.

Arndt, A., Schneider, C., 2023. Spatial pattern of glacier mass balance sensitivity to atmospheric forcing in High Mountain Asia. J. Glaciol. 1–18. https://doi.org/10.1017/jog.2023.46.

Arnold, M., Merchel, S., Bourlès, D.L., Braucher, R., Benedetti, L., Finkel, R.C., Aumaître, G., Gottdang, A., Klein, M., 2010. The French accelerator mass spectrometry facility ASTER: improved performance and developments Nuclear Instrumentation Methods. Physics Research Section B: Beam Interactions with Materials and Atoms 268, 1954–1959.

Ayache, M., Swingedouw, D., Mary, Y., Eynaud, F., Colin, C., 2018. Multi-centennial variability of the AMOC over the Holocene: a new reconstruction based on multiple proxy-derived SST records. Global Planet. Change 170, 173–183.

Balco, G., Stone, J.O., Lifton, N.A., Dunai, T.J., 2008. A complete and easily accessible means of calculating surface exposure ages or erosion rates from 10Be and 26Al measurements. Quat. Geochronol. 3 (3), 174–195.

Barandun, M., Pohl, E., 2022. Central Asia's spatiotemporal glacier response ambiguity due to data inconsistencies and regional simplifications. Cryosphere. https://doi.org/10.5194/tc-2022-117.

Barnard, P.L., Owen, L.A., Sharma, M.C., Finkel, R.C., 2004. Late quaternary holocene landscape evolution of a monsoon-influenced high himalayan valley, gori ganga, nanda devi, NE garhwal. Geomorphology 61, 91–110. https://doi.org/10.1016/j.geomorph.2003.12.002.

Barnard, P.L., Owen, L.A., Finkel, R.C., Asahi, K., 2006. Landscape response to deglaciation in a high relief, monsoon-influenced alpine environment, Langtang Himal, Nepal. Quat. Sci. Rev. 25, 2162–2176.

Benn, D.I., Owen, L.A., 2002. Himalayan glacial sedimentary environments: a framework for reconstructing and dating the former extent of glaciers in high mountains. Quat. Int. 97, 3–25. https://doi.org/10.1016/S1040-6182(02)00048-4.

Benn, D.I., Kirkbride, M.P., Owen, L.A., Brazier, V., 2003. Glaciated Valley Landsystems. Glacial Landsystems, pp. 372–406.

Benn, D.I., Bolch, T., Hands, K., Gulley, J., Luckman, A., Nicholson, L.I., Quincey, D., Thompson, S., Toumi, R., Wiseman, S., 2012. Response of debris-covered glaciers in the Mount Everest region to recent warming, and implications for outburst flood hazards. Earth Sci. Rev. 114 (1–2), 156–174. https://doi.org/10.1016/j.earscirev.2012.03.008.

Berthier, É., Brun, F., 2019. Karakoram geodetic glacier mass balances between 2008 and 2016: persistence of the anomaly and influence of a large rock avalanche on Siachen Glacier. J. Glaciol. 65, 494–507. https://doi.org/10.1017/jog.2019.32.

Bhardwaj, A., Joshi, P.K., Singh, M.K., Sam, L., Gupta, R.D., 2014. Mapping debris-covered glaciers and identifying factors affecting the accuracy. Cold Reg. Sci. Technol. 106, 161–174. https://doi.org/10.1016/j.coldregions.2014.07.006.

Bonekamp, P., de Kok, R., Collier, E., Immerzeel, W., 2019. Contrasting meteorological drivers of the glacier mass balance between the Karakoram and central Himalaya. Front. Earth Sci. 7. https://doi.org/10.3389/feart.2019.00107.

Bookhagen, B., Burbank, D.W., 2006. Topography, relief and TRMM-derived rainfall variations along the Himalaya. Geophys. Res. Lett. 33, L08405. https://doi.org/10.1029/2006GL026037.

Borchers, B., Marrero, S., Balco, G., Caffee, M., Goehring, B., Lifton, N., Nishiizumi, K., Phillips, F., Schaefer, J., Stone, J., 2016. Geological calibration of spallation production rates in the CRONUS-Earth project. Quat Geochro 31, 188–198.

Braucher, R., Guillou, V., Bourlès, D.L., Arnold, M., Aumaître, G., Keddadouche, K., Nottoli, E., 2015. Preparation of Aster in-house 10be/9be standard solutions. Nucl. Instrum. Methods Phys. Res. B 361, 335–340.

Brun, F., Berthier, E., Wagnon, P., Kääb, A., Treichler, D., 2017. A spatially resolved estimate of high mountain Asia glacier mass balances from 2000 to 2016. Nat. Geosci. 10, 668–673.

Brun, F., Wagnon, P., Berthier, E., Jomelli, V., Maharjan, S.B., Shrestha, F., Kraaijenbrink, P.D.A., 2019. Heterogeneous influence of glacier morphology on the mass balance variability in High Mountain Asia. JGR Earth Surface 124, 1–15.

Buri, P., Miles, E.S., Steiner, J.F., Immerzeel, W.W., Wagnon, P., Pellicciotti, F., 2016. A physically based 3-D model of ice cliff evolution over debris-covered glaciers. J. Geophys. Res. Earth Surf. 121, 2471–2493. https://doi.org/10.1002/2016JF004039.

Charton, J., Jomelli, V., Schimmelpfennig, I., Verfaillie, D., Favier, F., Mokadem, F., Gilbert, A., Brun, F., ASTER Team, 2020. Evolution of a debris-covered glacier (Gentil glacier) in Kerguelen archipelago (S°49, E°69) over the past 15,000 years constrained by ^{36}Cl CRE dating. Antarct. Sci. https://doi.org/10.1017/S0954102020000541.

Chmeleff, J., von Blanckenburg, F., Kossert, K., Jakob, D., 2010. Determination of the 10Be half-life by multicollector ICP-MS and liquid scintillation counting. Nucl. Instrum. Methods Phys. Res., Sect. B 268 (2), 192–199.

Compagno, L., Huss, M., Miles, E.S., McCarthy, M.J., Zekollari, H., Dehecq, A., Pellicciotti, F., Farinotti, D., 2022. Modelling supraglacial debris-cover evolution from the single-glacier to the regional scale: an application to High Mountain Asia. Cryosphere 16, 1697–1718. https://doi.org/10.5194/tc-16-1697-2022.

Delaney, I., Anderson, L.S., 2022. Debris cover limits subglacial erosion and promotes till accumulation. Geophys. Res. Lett. 49.

Deline, P., 2005. Change in surface debris cover on Mont Blanc massif glaciers after the'Little Ice Age' termination. Holocene 15, 302–309.

Fernández-Fernández, J.M., Palacios, D., García-Ruiz, J.M., Andrés, N., Schimmelpfennig, I., Gómez-Villar, A., Santos-González, J., Álvarez-Martínez, J., Úbeda, J., Léanni, L., ASTER Team, 2017. Chronological and geomorphological investigation of fossil debris-covered glaciers in relation to deglaciation processes: A case study in the Sierra de La Demanda, northern Spain. Quat. Sci. Rev. 170, 232–249.

Finkel, R.C., Owen, L.A., Barnard, P.L., Caffee, M.W., 2003. Beryllium-10 dating of Mount Everest moraines indicates a strong monsoonal influence and glacial synchroneity throughout the Himalaya. Geology 31, 561–564.

Fletcher, W.J., Sanchez Goni M, F., Naughton, F., Sepp, H., 2023. Northgrippian stage (middle holocene, 8.2-4.2 ka). In: Palacios, D., Hughes, P.D., Jomelli, V., Tanarro, L. M. (Eds.), Chap 7 in European Glacial Landscapes, the Holocene. Elsevier, pp. 89–99. ISBN 978-0-323-99712-6.

Fugger, S., Fyffe, C.L., Fatichi, S., Miles, E., McCarthy, M., Shaw, T.E., Ding, B., Yang, W., Wagnon, P., Immerzeel, W., Liu, Q., Pellicciotti, F., 2022. Understanding monsoon control on the energy and mass balance in the Central and Eastern Himalaya. Cryosphere 16, 1631–1652. https://doi.org/10.5194/tc-16-1631-2022.

Gardelle, J., Berthier, E., Arnaud, Y., 2012. Impact of resolution and radar penetration on glacier elevation changes computed from multi-temporal DEMs. J. Glaciol. 58, 419–422.

Gibson, M.J., Glasser, N.F., Quincey, D.J., Mayer, C., Rowan, A.V., Irvine-Fynn, T.D., 2017. Temporal variations in supraglacial debris distribution on Baltoro Glacier, Karakoram between 2001 and 2012. Geomorphology 295, 572–585. https://doi.org/10.1016/j.geomorph.2017.08.012.

Giese, A., Boone, A., Wagnon, P., Hawley, R., 2020. Incorporating moisture content in surface energy balance modeling of a debris-covered glacier. Cryosphere 14, 1555–1577. https://doi.org/10.5194/tc-14-1555-2020, 2020.

Guha, S., Tiwari, R.K., 2023. Analyzing geomorphological and topographical controls for the heterogeneous glacier mass balance in the Sikkim Himalayas. J. Mt. Sci. 26, 1854, 64.

Hambrey, M.J., Quincey, D.J., Glasser, N.F., Reynolds, J.M., Richardson, S.J., Clemmens, S., 2008. Sedimentological, geomorphological and dynamic context of debris-mantled glaciers, Mount Everest (Sagarmatha) region, Nepal. Quat. Sci. Rev. 27, 2361–2389. https://doi.org/10.1016/j.quascirev.2008.08.010.

Hedrick, K.A., Seong, Y.B., Owen, L.A., Caffee, M.W., Dietsch, C., 2011. Towards defining the transition in style and timing of Quaternary glaciation between the monsoon-influenced Greater Himalaya and the semi-arid Transhimalaya of Northern. India. Quat. Int. 236, 21–33.

Herreid, S., Pellicciotti, F., 2020. The state of rock debris covering Earth's glaciers. Nat Geoscience. Nat. Geosci. 13, 621–627.

Hornsey, J., Rowan, A.V., Kirkbride, M., Livingstone, S.T., Fabel, D., Rodes, A., Quincey, D.J., Hubbard, B., Jomelli, V., 2022. Be-10 dating of ice-marginal moraines in the Khumbu Valley, Nepal, Central Himalaya, reveals the response of monsoon-influenced debris-covered glaciers to Holocene climate change. JGR 127. https://doi.org/10.1029/2022JF006645.

Huss, M., Funk, M., Ohmura, A., 2009. Strong Alpine glacier melt in the 1940s due to enhanced solar radiation. Geophys. Res. Lett. 36, L23501.

IPCC SROCC, 2019. The Ocean and Cryosphere in a Changing Climate. Cambridge University Press, Cambridge, UK and New York, NY, USA, pp. 131–202. https://doi.org/10.1017/9781009157964.004.

Jóhannesson Raymond, C., Waddington, E., 1989. Timescale for adjustment of glaciers to changes in mass balance. J. Glaciol. 35, 355–369.

Jomelli, V., Francou, B., 2000. Comparing characteristics of rockfall talus and snow avalanche landforms in an alpine environment using a new methodological approach. Geomorphology 35, 181–192.

Jomelli, V., Swingedouw, D., Vuille, M., Favier, V., Goehring, B., Shakun, J., Braucher, R., Schimmelpfennig, I., Menviel, L., Rabatel, A., Martin, L.C.P., Blard, P.-H., Condom, T., Lupker, M., Christl, M., He, Verfaillie, D.Z., Gorin, A., ASTER Team, 2022. AMOC control on millennial-scale glacier changes during the Holocene. Nature com. https://doi.org/10.1038/s41467-022-28939-9.

Jomelli, V., Wagnon, P., Swingedouw, D., Charton, J., Braucher, R., Hue, A., Brun, F., Shrestha, D., Aster TEAM, 2023. Unraveling the climate control on debris-free glacier evolution in the Everest region (Nepal, Central Himalaya) during the Holocene. QSR. https://doi.org/10.1016/j.quascirev.2023.108109.

Kääb, A., Berthier, E., Nuth, C., Gardelle, J., Arnaud, Y., 2012. Contrasting patterns of early twenty-first-century glacier mass change in the Himalayas. Nature 488, 495–498.

Khadka, A., Matthews, T., Perry, L.B., Koch, I., Wagnon, P., Shrestha, D., Sherpa, T.C.G., Aryal, D., Tait, A., Sherpa, T.C.G., Tuladhar, S., Baidya, S.K., Elvin, S., Elmore, A.C., Gajurel, A., Mayewski, P.A., 2021. Weather on mount everest during the 2019 summer monsoon. Weather 76, 205–207. https://doi.org/10.1002/wea.3931.

Khadka, A., Wagnon, P., Brun, F., Shrestha, D., Lejeune, Y., Arnaud, Y., 2022. Evaluation of ERA5-Land and HARv2 reanalysis data at high elevation in the upper Dudh Koshi basin (Everest region, Nepal). J. Appl. Meteorol. Climatol. 61, 931–954. https://doi.org/10.1175/jamc-d-21-0091.1.

Khadka, A., Brun, F., Wagnon, P., Shrestha, D., Sherpa, T., 2024. Surface energy and mass balance of Mera Glacier in the Everest region (Nepal, Central Himalaya) and their sensitivity to temperature and precipitation. J. Glaciol. https://doi.org/10.31223/X50415.

Kirkbride, M.P., 1993. The temporal significance of transitions from melting to calving termini at glaciers in the central Southern Alps of New Zealand. Holocene 3 (3), 232–240. https://doi.org/10.1177/095968369300300305.

Korschinek, G., Bergmaier, A., Faestermann, T., Gerstmann, U.C., Knie, K., Rugel, G., Wallner, A., Dillmann, I., Dollinger, G., von Gostomski, ChL., Kossert, K., Maiti, M., Poutivtsev, M., Remmert, A., 2010. A new value for the half-life of ^{10}Be by Heavy-Ion Elastic Recoil Detection and liquid scintillation counting. Nucl. Instrum. Methods Phys. Res. Sect. B Beam Interact. Mater. Atoms 268 (2), 187–191. https://doi.org/10.1016/j.nimb.2009.09.020.

Lal, D., 1991. Cosmic ray labeling of erosion surfaces: in situ nuclide production rates and erosion models. Earth Planet Sci. Lett. 104, 424–439. https://doi.org/10.1016/0012-821X(91)90220-C.

Lifton, N., Sato, T., Dunai, T.J., 2014. Scaling in situ cosmogenic nuclide production rates using analytical approximations to atmospheric cosmic-ray fluxes. Earth Planet Sci. Lett. 386, 149–160. https://doi.org/10.1016/j.epsl.2013.10.052.

Litt, M., Shea, J., Wagnon, P., Steiner, J., Koch, I., Stigter, E., Immerzeel, W., 2019. Glacier ablation and temperature indexed melt models in the nepalese himalaya. Sci. Rep. 9 (1), 1–10.

Martin, L.C.P., Blard, P.-H., Balco, G., Lave, J., Delunel, R., Lifton, N., Laurent, V., 2017. The CREp program and the ICE-D production rate calibration database: a fully parameterizable and updated online tool to compute cosmic-ray exposure ages. Quat. Geochronol. 38, 25–49.

Matthews, T., Perry, L.B., Koch, I., Aryal, D., Khadka, A., Shrestha, D., Abernathy, K., Elmore, A.C., Seimon, A., Tait, A., Elvin, S., Tuladhar, S., Baidya, S.K., Potocki, M.,

Kang, S.D., Sherpa, T.C., Gajurel, A., Mayewski, P.A., 2020. Going to Extremes: Installing the World's Highest Weather Stations on Mount Everest, vol. 101. BAMS, pp. 1870–1890.
Mayer, J.M., Lambrecht, C., Wirbel, A., Kueppers, U., 2013. Thermal properties of a supraglacial debris layer with respect to lithology and grain size. Geogr. Ann. Phys. Geogr. 95 (3), 197–209. https://doi.org/10.1111/geoa.12011.
McCarthy, M., Miles, E., Kneib, M., Buri, P., Fugger, S., Pellicciotti, F., 2021. Supraglacial debris thickness and supply rate in High Mountain Asia. Communications Earth and Environment. https://doi.org/10.31223/X5WW5B.
Merchel, S., Bremser, W., Alfimov, V., Arnold, M., Aumaître, G., Benedetti, L., Bourles, D. L., Caffee, M., Fifield, L.K., Finkel, R.C., Freeman, S.P.H.T., Martschini, M., Matsushi, Y., Rood, D.H., Sasa, K., Steier, P., Takahashi, T., Tamari, M., Tims, S.G., Tosaki, Y., Wilcken, K.M., Xu, S., 2011. Ultra-trace analysis of ^{36}Cl by accelerator mass spectrometry: an interlaboratory study. Anal. Bioanal. Chem. Res. 400, 3125–3132.
Miles, E.S.Pellicciotti, Willis, F., Steiner, I.C., Buri, J.F., Arnold N.S, P., 2016. Refined energy-balance modelling of a supraglacial pond. Langtang Khola, Nepal Ann. Glaciol. https://doi.org/10.3189/2016AoG71A421, 2016.
Mölg, N., Bolch, T., Walter, A., Vieli, A., 2019. Unravelling the evolution of zmuttgletscher and its debris cover since the end of the Little ice age. Cryosphere 13, 1889–1909. https://doi.org/10.5194/tc-13-1889-2019.
Murari, M.K., Owen, L.A., Dortch, J.M., Caffee, M.W., Dietsch, C., Fuchs, M., Haneberg, W.C., Sharma, M.C., Townsend-Small, A., 2014. Timing and climatic drivers for glaciation across monsoon-influenced regions of the Himalayane Tibetan orogen. Quat. Sci. Rev. 88, 159–182.
Nakawo, M., Yabuki, H., Sakai, A., 1999. Characteristics of Khumbu glacier, Nepal Himalaya: recent change in the debris-covered area. Annal of Glacio 28, 118–122.
Nicholson, L., Benn, D.I., 2006. Calculating ice melt beneath a debris layer using meteorological data. J. Glaciol. 52 (178), 463–470, 10. 3189/172756506781828584.
Nicholson, L.I., McCarthy, M., Pritchard, H.D., Willis, I., 2018. Supraglacial debris thickness variability: impact on ablation and relation to terrain properties. Cryosphere 12, 3719–3734. https://doi.org/10.5194/tc-12-3719-2018.
Nuimura, T., Fujita, K., Yamaguchi, S., Sharma, R.R., 2012. Elevation changes of glaciers revealed by multitemporal digital elevation models calibrated by GPS survey in the Khumbu region, Nepal Himalaya, 1992-2008. J. Glaciol. 58 (210), 648–656.
Osti, R., Egashira, S., 2009. Hydrodynamic characteristics of the Tam Pokhari glacial lake outburst flood in the Mt. Everest region, Nepal. Hydrol. Process. 23, 2943–2955. https://doi.org/10.1002/hyp.7405.
Østrem, G., 1959. Ice melting under a thin layer of moraine and the existence of ice cores in moraine ridges. Geogr. Ann. 41 (4), 228–230.
Owen, L.A., 2009. Latest pleistocene and holocene glacier fluctuations in the Himalaya and Tibet. Quat. Sci. Rev. 28, 2150–2164.
Owen, L.A., Benn, D.I., 2005. Equilibrium-line altitudes of the last glacial maximum for the himalaya and Tibet: an assessment and evaluation of results. Quat. Int. 138/139, 55–78.
Owen, L.A., Dortch, J.M., 2014. Nature and timing of Quaternary glaciation in the Himalayan Tibetan orogen. Quat. Sci. Rev. 88, 14–54.
Owen, L.A., Finkel, R.C., Barnard, P.L., Haizhou, M., Asahi, K., Caffee, M.W., Derbyshire, E., 2005. Climatic and topographic controls on the style and timing of Late Quaternary glaciation throughout Tibet and the Himalaya defined by10Be cosmogenic radionuclide surface exposure dating. Quat. Sci. Rev. 24, 1391–1411.
Owen, L.A., Caffee, M.W., Finkel, R.C., Seong, B.Y., 2008. Quaternary glaciations of the Himalayan Tibetan orogen. J. Quat. Sci. 23, 513–532.
Owen, L.A., Robinson, R., Benn, D.I., Finkel, R.C., Davis, N.K., Yi, C., Putkonen, J., Li, D., Murray, A.S., 2009. Quaternary glaciation of mount everest. Quat. Sci. Rev. 28, 1412–1433.
Perry, L.B., Matthews, T., Guy, H., Koch, I., Khadka, A., Elmore, A.C., Shrestha, D., Tuladhar, S., Baidya, S.K., Maharjan, S., Wagnon, P., Aryal, D., Seimon, A., Gajurel, A., Mayewski, P.A., 2020. Precipitation characteristics and moisture source regions on Mt. Everest in the Khumbu, Nepal. One Earth 3, 594–607.
Rowan, A.V., 2017. The 'Little Ice Age' in the Himalaya: a review of glacier advance driven by Northern Hemisphere temperature change. Holocene 27, 292–308.
Rowan, A., Egholm, L., Quincey, J., Glasser, F., 2015. Modelling the feedbacks between mass balance, ice flow and debris transport to predict the response to climate change of debris-covered glaciers in the Himalaya. Earth Planet Sci. Lett. 430, 427–438. https://doi.org/10.1016/j.epsl.2015.09.004.
Saha, S., Owen, L.A., Orr, E.N., Caffee, M.W., 2018. Timing and nature of Holocene glacier advances at the northwesternend of the Himalayan-Tibetan orogen. Quat. Sci. Rev. 187, 177–202.
Saha, S., Owen, L.A., Orr, E.N., Caffee, M.W., 2019a. Cosmogenic 10be and equilibrium-line altitude dataset of holocene glacier advances in the himalayan-Tibetan orogen. Data Brief 26, 104412. https://doi.org/10.1016/j.dib.2019.104412.
Saha, S., Owen, L.A., Orr, E.N., Caffee, M.W., 2019b. High-frequency Holocene glacier fluctuations in the Himalayan Tibetan orogen. Quat. Sci. Rev. 220, 372–400.
Sakaï, A., Fujita, K., 2017. Contrasting glacier responses to recent climate change in high mountain Asia. Sci. Rep. 7, 13717. https://doi.org/10.1038/s41598-017-14256-5.
Sakai, A., Nakawo, M., Fujita, K., 2002. Distribution characteristics and energy balance of ice cliffs on debris-covered glaciers, Nepal himalaya. Arctic, Antarct. Alp. Res. 34, 12–19.
Scherler, D., Bookhagen, B., Strecker, M.R., 2011. Spatially variable response of Himalayan glaciers to climate change affected by debris cover. Nat. Geosci. 4 (3), 156–159. https://doi.org/10.1038/ngeo1068.
Scherler, D., Wulf, H., Gorelick, N., 2018. Global assessment of supraglacial debris-cover extents. Geophys. Res. Lett. 45 (21), 11–798, 10. 1029/2018GL080158.
Schimmelpfennig, I., Schaefer, J.M., Lamp, J., Godard, V., Schwartz, R., Bard, E., et al., 2022. Glacier response to Holocene warmth inferred from in situ 10Be and 14C bedrock analyses in Steingletscher's forefield (central Swiss Alps). Clim. Past 18, 23–44.
Seong, Y.B., Owen, L.A., Bishop, M.P., Bush, A., Clendon, P., Copland, L., Finkel, R., Kamp, U., Shroder, J.F., 2007. Quaternary glacial history of the central Karakoram. Quat. Sci. Rev. 26, 3384–3405.
Seong, Y, B., Owen, L.A., Yi, C., Finkel, R., 2009. Quaternary glaciation of Muztag Ata and Kongur Shan: evidence for glacier response to rapid climate changes throughout the late glacial and holocene in westernmost Tibet. GSA Bulletin 121 (3/4), 348–365. https://doi.org/10.1130/B26339.1. March/April 2009.
Sherpa, S.F., Wagnon, P., Brun, F., Berthier, E., Vincent, C., Lejeune, Y., Arnaud, Y., Kayastha, R., Sinisalo, A., 2017. Contrasted surface mass balances of debris-free glaciers observed between the southern and the inner parts of the Everest region (2007-2015). J. Glaciol. https://doi.org/10.1017/jog.2017.30.
Shokory, J.A.N., Lane, S.N., 2023. Patterns and drivers of glacier debris-cover development in the Afghanistan Hindu Kush Himalaya. J. Glaciol. 1–15. https://doi.org/10.1017/jog.2023.1.
Solomina, O.N., Bradley, R.S., Hodgson, D.A., Ivy-Ochs, S., Jomelli, V., Mackintosh, A.N., Nesje, A., Owen, L.A., Wanner, H., Wiles, G.C., Young, N.E., 2015. Holocene glacier fluctuations. Quat. Sci. Rev. 111, 9–34.
Solomina, O., Bradley, Jomelli, V., Geirsdottir, A., Kaufman, D., Koch, J., Masiokas, M., Miller, G., Nesje, A., Nicolussi, K., Owen, L., Wanner, H., Wiles, G., Yang, B., 2016. Glacier fluctuations in the last 2000 years. Quat. Sci. Rev. 149, 61–90.
Stigter, E.E., Litt, M., Steiner, J.F., Bonekamp, P.N.J., Shea, J.M., Bierkens, M.F.P., Immerzeel, W.W., 2018. The importance of snow sublimation on a himalayan glacier. Front. Earth Sci. 6|. https://doi.org/10.3389/feart.2018.00108.
Stigter, E.E., Steiner, J.F., Koch, I., Saloranta, T.M., Kirkham, J.D., Immerzeel, W.W., 2021. Energy and mass balance dynamics of the seasonal snowpack at two high-altitude sites in the Himalaya. Cold Reg. Sci. Technol. 183. https://doi.org/10.1016/j.coldregions.2021.103233.
Stone, J.O., 2000. Air pressure and cosmogenic isotope production. J. Geophys. Res. Solid Earth 105 (B10), 23753–23759. https://doi.org/10.1029/2000JB900181.
Takeuchi, Y., Kayastha, R.B., Nakawo, M., 2000. Characteristics of Ablation and Heat Balance in Debris-free and Debris-Covered Areas on Khumbu Glacier, Nepal Himalayas, in the Pre-monsoon Season. Debris-Covered Glaciers (Proceedings of a Workshop Held at Seattle, Washington, USA, September 2000). IAHS Publ no. 264, 2000.
Tanarro, L.M., Palacios, D., Fernández-Fernández, J.M., Andrés, N., Oliva, M., Rodríguez-Mena, M., Schimmelpfennig, I., Brynjólfsson, S., Sæmundsson, þ., Zamorano, J.J., Jose Úbeda, J., ASTER Team, 2021. Origins of the divergent evolution of mountain glaciers during deglaciation: hofsdalur cirques, Northern Iceland. Quat. Sci. Rev. 273. https://doi.org/10.1016/j.quascirev.2021.107248.
Thompson, L.G., Tao, T., Davis, M.E., Henderson, A., Mosley-Thompson, E., Lin, P.N., Beer, J., Synal, H.A., Cole-Dai, J., Bolzan, J.F., 1997. Tropical climate instability: the last glacial cycle from a Qinghai- Tibetan ice core. Science 276, 1821–1825.
Thornalley, D.J.R., Blaschek, M., Davies, F.J., Praetorius, S., Oppo, D.W., McManus, J.F., Hall, I.R., Kleiven, H., Renssen, H., McCave, I.N., 2013. Long-term variations in Icelande Scotland overflow strength during the holocene geoscientific instrumentation methods and data systems. Clim. Past 9, 2073–2084.
Tielidze, L.G., Bolch, T., Wheate, R.D., Kutuzov, S.S., Lavrentiev, I.I., Zemp, M., 2020. Supra-glacial debris cover changes in the Greater Caucasus from 1986 to 2014. Cryosphere 14, 585–598. https://doi.org/10.5194/tc-14-585-2020.
Uppala, S.M., Kållberg, P.W., Simmons, A.J., Andrae, U., Bechtold, V.D.C., Fiorino, M., Gibson, J.K., Haseler, J., Hernandez, A., Kelly, G.A., Li, X., Onogi, K., Saarinen, S., Sokka, N., Allan, R.P., Andersson, E., Arpe, K., Balmaseda, M.A., Beljaars, A.C.M., Berg, L.V.D., Bidlot, J., Bormann, N., Caires, S., Chevallier, F., Dethof, A., Dragosavac, M., Fisher, M., Fuentes, M., Hagemann, S., Hólm, E., Hoskins, B.J., Isaksen, L., Janssen, P.A.E.M., Jenne, R., Mcnally, A.P., Mahfouf, J.-F., Morcrette, J.-J., Rayner, N.A., Saunders, R.W., Simon, P., Sterl, A., Trenberth, K.E., Untch, A., Vasiljevic, D., Viterbo, P., Woollen, J., 2005. The ERA-40 re-analysis. Q. J. R. Meteorol. Soc. 131, 2961–3012.
Wagnon, P., Vincent, C., Arnaud, Y., Berthier, E., Vuillermoz, E., Gruber, S., Ménégoz, M., Gilbert, A., Dumont, M., Shea, J.M., Stumm, D., Pokhrel, B.K., 2013. Seasonal and annual mass balances of mera and pokalde glaciers (Nepal himalaya) since 2007. Cryosphere 7 (6), 1769–1786, 2013.
Wagnon, P., Brun, F., Khadka, A., Berthier, A., Shrestha, E., Vincent, D., Arnaud, C., Six, Y., Dehecq, A, D., Ménégoz, M., Jomelli, V., 2021. Reanalysing the 2007–19 glaciological mass-balance series of mera glacier, Nepal, central Himalaya, using geodetic mass balance. J. Glaciol. 67, 117–125.
Ward, G.K., Wilson, S.R., 1978. Procedures for comparing and combining radiocarbon age determinations: a critique. Archaeometry 20, 19–31.
Winter-billington, A., Dadic, R., Moore, R.D., Flerchinger, G., Wagnon, P., Banerjee, A., 2022. Modelling debris-covered glacier ablation using the simultaneous heat and water transport model. Part 1: model Development and Application to North Changri Nup. Front. Earth Sci. 10–2022. https://doi.org/10.3389/feart.2022.796877.
Yu, Z., Colin, C., Wilson, D.J., Bayon, G., Song, Z., Sepulcre, S., Dapoigny, A., Li, Y., Wan, S., 2022. Millennial variability in intermediate ocean circulation and Indian monsoonal weathering inputs during the last deglaciation and Holocene. Geophys. Res. Lett. 49, e2022GL100003. https://doi.org/10.1029/2022GL100003.